

Experimental and Computational Studies of the Isomerization Reactions of Bidentate Phosphine Ligands in Triosmium Clusters: Kinetics of the Rearrangements from Bridged to Chelated Isomers and X-ray Structures of the Clusters $\text{Os}_3(\text{CO})_{10}(\text{dppbz})$, $1,1\text{-Os}_3(\text{CO})_{10}(\text{dppbzF}_4)$, $\text{HOs}_3(\text{CO})_9[\mu\text{-}1,2\text{-PhP}(\text{C}_6\text{H}_4\text{-}\eta^1)\text{C}_6\text{H}_4\text{PPh}_2]$, and $\text{HOs}_3(\text{CO})_9[\mu\text{-}1,2\text{-PhP}(\text{C}_6\text{H}_4\text{-}\eta^1)\text{C}_6\text{F}_4\text{PPh}_2]$

Xue Zhang,^{†,‡} Srikanth Kandala,[†] Li Yang,[†] William H. Watson,[§] Xiaoping Wang,^{||} David A. Hrovat,^{†,‡} Weston Thatcher Borden,^{*,†,‡} and Michael G. Richmond^{*,†}

[†]Department of Chemistry and [‡]Center for Advanced Scientific Computing and Modeling, University of North Texas, Denton, Texas 76203-5017, United States, [§]Department of Chemistry, Texas Christian University, Fort Worth, Texas 76129, United States, and ^{||}Neutron Scattering Science Division, Oak Ridge National Laboratory, Oak Ridge, Tennessee 37831, United States

Received August 11, 2010

The diphosphine ligand 1,2-bis(diphenylphosphino)benzene (dppbz) reacts with the activated cluster $1,2\text{-Os}_3(\text{CO})_{10}(\text{MeCN})_2$ (**1**) at room temperature to furnish a mixture of the triosmium clusters $1,2\text{-Os}_3(\text{CO})_{10}(\text{dppbz})$ (**2**) and $1,1\text{-Os}_3(\text{CO})_{10}(\text{dppbz})$ (**3**), along with a trace amount of the hydride cluster $\text{HOs}_3(\text{CO})_9[\mu\text{-}1,2\text{-PhP}(\text{C}_6\text{H}_4\text{-}\eta^1)\text{C}_6\text{H}_4\text{PPh}_2]$ (**4**). The dppbz-bridged cluster **2** forms as the kinetically controlled product and irreversibly transforms to the corresponding chelated isomer **3** at ambient temperature. The disposition of the dppbz ligand in **2** and **3** has been established by X-ray crystallography and ³¹P NMR spectroscopy, and the kinetics for the conversion **2** → **3** have been followed by UV–vis spectroscopy in toluene over the temperature range 318–343 K. The calculated activation parameters ($\Delta H^\ddagger = 21.6(3)$ kcal/mol; $\Delta S^\ddagger = -11(1)$ eu) and lack of CO inhibition support an intramolecular isomerization mechanism that involves the simultaneous migration of phosphine and CO groups about the cluster polyhedron. The reaction between **1** and the fluorinated diphosphine ligand 1,2-bis(diphenylphosphino)tetrafluorobenzene (dppbzF₄) was examined under similar reaction conditions and was found to afford the chelated cluster $1,1\text{-Os}_3(\text{CO})_{10}(\text{dppbzF}_4)$ (**6**) as the sole observable product. The absence of the expected bridged isomer $1,2\text{-Os}_3(\text{CO})_{10}(\text{dppbzF}_4)$ (**5**) suggests that the dppbzF₄ ligand destabilizes **5**, thus accounting for the rapid isomerization of **5** to **6**. Near-UV irradiation of clusters **3** and **6** leads to CO loss and ortho metalation of an ancillary aryl group. The resulting hydride clusters **4** and $\text{HOs}_3(\text{CO})_9[\mu\text{-}1,2\text{-PhP}(\text{C}_6\text{H}_4\text{-}\eta^1)\text{C}_6\text{F}_4\text{PPh}_2]$ (**7**) have been isolated and fully characterized by spectroscopic and X-ray diffraction analyses. Both **4** and **7** react with added CO under mild conditions to regenerate **3** and **6**, respectively, in quantitative yield. The rearrangements of bridged to chelated diphosphine complexes in this genre of decacarbonyl clusters have been investigated by DFT calculations. The computational results support a concerted process, involving the scrambling of equatorial CO and phosphine groups via a classical merry-go-round exchange scheme. The barriers computed for this mechanism agree well with those that have been measured, and steric compression within the bridged diphosphine groups of the reactants has been calculated to reduce the barrier heights for the rearrangement.

Introduction

Ligand fluxionality in polynuclear metal compounds is a well-established phenomenon. Numerous reports that unequivocally demonstrate the nonrigidity of CO, NO, RNC, and hydride ligands may be found in the chemical literature dating back to the 1960s.¹ In the absence of a ligand

dissociation/association process (i.e. ligand on, ligand off),² the permutation of a terminally bound (η^1) ligand(s) between

*To whom correspondence should be addressed. W.T.B.: tel, 940-565-3658; e-mail, borden@unt.edu. M.G.R.: tel, 940-565-3548; e-mail, cobalt@unt.edu.

(1) (a) Cotton, F. A.; Kruczynski, L.; Shapiro, B. L.; Johnson, L. F. *J. Am. Chem. Soc.* **1972**, *94*, 6191. (b) Adams, R. D.; Cotton, F. A. In *Dynamic Nuclear Magnetic Resonance Spectroscopy*; Jackman, L. M., Cotton, F. A., Eds.; Academic Press: New York, 1975; Chapter 12. (c) Farrugia, L. J. *Dalton Trans.* **1997**, 1783. (d) Green, M.; Mead, K. A.; Mills, R. M.; Salter, I. D.; Stone, F. G. A.; Woodward, P. *Chem. Commun.* **1982**, 51. (e) Musaev, D. G.; Nowroozi-Isfahani, T.; Morokuma, K.; Abedin, J.; Rosenberg, E.; Hardcastle, K. I. *Organometallics* **2006**, *25*, 203.

different metal centers is assumed to proceed via an intermediate or transition structure, involving the simultaneous coordination of the ligand to two or more metal centers. The exact degree of ligand bridging depends upon the nuclearity of the metallic ensemble and the energetics of ligand exchange.³ The bulk of the published studies of intramolecular scrambling of an ancillary ligand(s) about a metal cluster indicate at least one terminal–bridge–terminal transposition of the migratory ligand(s). These ligands exhibit a high degree of coordinative flexibility, and they display a gamut of bonding modes from terminal (η^1) to multisite, face-capping (μ_4) coordination.^{3,4}

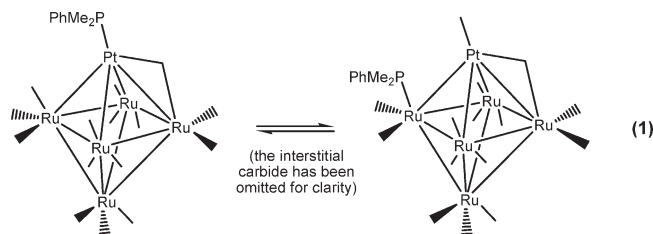
Tertiary phosphine and phosphite ligands are regarded as good σ donors and they can also function as π -acceptor ligands, depending upon the nature of the ancillary substituents.⁵ Historically, such pnictogen ligands have been assumed to serve as terminal or η^1 ligands, and their coordination chemistry has been assumed to be restricted to a single metal site, irrespective of the nuclearity of the compound.⁶ This provincial view, in which a phosphine acts as a 2e donor through electron-precise bonding to only a single metal center, has recently been challenged, and crystallographic and solution NMR data have provided irrefutable confirmation for the ligation of two or more metal centers by PF_3 and PR_3 ligands.

The first structural demonstration of nontraditional bonding between a tertiary phosphine and a polynuclear cluster may be traced to the study by Balch of the reaction of $\text{Pd}_2(\mu\text{-dppm})_2\text{Cl}_2$ with PF_3 , which affords the trinuclear cluster $[\text{Pd}_3(\mu_3\text{-PF}_3)(\mu\text{-Cl})(\mu\text{-dppm})_3]^+$.⁷ The capping of one of the triangular faces in the Pd_3 cluster by the ancillary PF_3 ligand defies description within a valence-bond perspective. An electron-deficient or delocalized model of bonding is required in order to describe the interaction involving the metallic core and the ancillary PF_3 ligand.⁸ Other notable structures, containing dimetallic motifs that are bridged by a tertiary phosphine group(s), have been reported by the Werner and Réau groups.^{9,10}

The bridging-to-chelating isomerization of the diphosphine ligand in $\text{H}_4\text{Ru}_4(\text{CO})_{10}(\text{dppe})$, discovered by Shapley and Churchill, represents the first demonstrable example of a

coordinatively flexible, ancillary phosphine ligand in a polynuclear cluster.¹¹ A subsequent kinetic investigation provided compelling evidence for a nondissociative mechanism for the migration of the dppe ligand in the Ru_4 cluster.¹² Other early examples involving phosphine fluxionality in di- and trimetallic compounds have been reported, and these include the reversible migration of phosphine ligands about the triangular Pt_3 face of $[\text{Pt}_3(\mu_3\text{-CO})\text{P}(\mu\text{-dppm})_3]^{2+}$ (where P = monodentate phosphine, phosphite) and the “end-over-end” exchange of one of the bridging diphosphine ligands in the compounds $[\text{Ag}_2(\text{dppm})_3]^{2+}$, $[\text{Ag}_2(\text{dmpm})_3]^{2+}$, and $[\text{Ag}_2(\text{dppm})_{3-x}(\text{dmpm})_x]^{2+}$ (where $x = 1, 2$).^{13–16}

In 2000, Adams presented landmark evidence for the intramolecular exchange of the PMe_2Ph ligand about platinum and ruthenium sites in the heterometallic cluster $\text{PtRu}_5(\mu_6\text{-C})(\text{CO})_{15}(\text{PMe}_2\text{Ph})$, as depicted in eq 1.^{17,18} The scrambling of the phosphine ligand about the cluster polyhedron was investigated by VT NMR measurements, and ¹⁹⁵Pt satellites for the different PMe_2Ph isomers were observed throughout the exchange process. This latter feature is important, as it eliminates an isomerization process arising from a ligand dissociation/association scenario.¹⁹ A mechanism involving a $\mu_2\text{-PMe}_2\text{Ph}$ intermediate, coupled with a series of CO shifts across Pt–Ru and Ru–Ru bonds, was proposed for the dynamic isomerization that leads to the equilibration of the phosphine ligand between the different metal centers.



(11) Churchill, M. R.; Lashewycz, R. A.; Shapley, J. R.; Richter, S. I. *Inorg. Chem.* **1980**, *19*, 1277.

(12) Kandala, S.; Richmond, M. G. *Inorg. Chem.* **2006**, *45*, 5976.

(13) (a) Bradford, A. M.; Jennings, M. C.; Puddephatt, R. J. *Organometallics* **1988**, *7*, 792. (b) Bradford, A. M.; Douglas, G.; Manojlović-Muir, L.; Muir, K. W.; Puddephatt, R. J. *Organometallics* **1990**, *9*, 409.

(14) Dean, P. A. W.; Vittal, J. J.; Srivastava, R. S. *Can. J. Chem.* **1987**, *65*, 2628.

(15) For some additional early reports that address the dynamic fluxionality of different pnictogen-based ligands at polynuclear systems, see: (a) Sutin, K. A.; Kolis, J. W.; Mlekuz, M.; Bougeard, P.; Sayer, B. G.; Quilliam, M. A.; Faggiani, R.; Lock, C. J. L.; McGlinchey, M. J.; Jaouen, G. *Organometallics* **1987**, *6*, 439. (b) Deeming, A. J.; Smith, M. B. *Dalton Trans.* **1993**, 3383. (c) Yang, K.; Smith, J. M.; Bott, S. G.; Richmond, M. G. *Organometallics* **1993**, *12*, 4779. (d) Yang, K.; Bott, S. G.; Richmond, M. G. *Organometallics* **1994**, *13*, 3788. (e) Laurency, G.; Bondietti, G.; Ros, R.; Roulet, R. *Inorg. Chim. Acta* **1996**, *247*, 65.

(16) For a related report describing the chelate \rightarrow bridge isomerization of the dppe ligands in $\text{Mo}_2\text{Br}_4(\text{dppe})_2$ that proceeds via the internal rotation of the Mo_2 moiety within the cubic cage of the ancillary ligands, see: Agaskar, P. A.; Cotton, F. A.; Derringer, D. R.; Powell, G. L.; Root, D. R.; Smith, T. J. *Inorg. Chem.* **1985**, *24*, 2786.

(17) (a) Adams, R. D.; Captain, B.; Fu, W.; Pellechia, P. J. *Chem. Commun.* **2000**, 937. (b) *ibid.* *Inorg. Chem.* **2003**, *42*, 3111.

(18) For other relevant studies dealing with the fluxionality of a phosphine ligand at di- and polynuclear systems: (a) Ohki, Y.; Suzuki, H. *Angew. Chem., Int. Ed.* **2002**, *41*, 2994. (b) Gallo, V.; Mastroilli, P.; Nobile, C. F.; Braunstein, P.; Englert, U. *Dalton Trans.* **2006**, 2343. (c) Begum, N.; Das, U. K.; Hassan, M.; Hogarth, G.; Kabir, S. E.; Nordlander, E.; Rahman, M. A.; Tocher, D. A. *Organometallics* **2007**, *26*, 6462. (d) Esswein, A. J.; Veige, A. S.; Piccoli, P. M. B.; Schultz, A. J.; Nocera, D. G. *Organometallics* **2008**, *27*, 1073.

(2) For ligand substitution reactions involving dissociative and associative manifolds, see: (a) Vanni, H.; Merbach, A. E. *Inorg. Chem.* **1979**, *18*, 2758. (b) Kowaleski, R. M.; Basolo, F.; Trogler, W. C.; Ernst, R. D. *J. Am. Chem. Soc.* **1986**, *108*, 6046. (c) Turaki, N. N.; Huggins, J. M.; Lebioda, L. *Inorg. Chem.* **1988**, *27*, 424.

(3) Band, E.; Muettterties, E. L. *Chem. Rev.* **1978**, *78*, 639.

(4) Johnson, B. F. G.; Rodgers, A. In *The Chemistry of Metal Cluster Complexes*; Shriver, D. F., Kaesz, H. D., Adams, R. D., Eds.; VCH: New York, 1990; Chapter 6.

(5) Orpen, A. G.; Connelly, N. G. *Chem. Commun.* **1985**, 1310.

(6) Braunstein, P.; Boag, N. M. *Angew. Chem., Int. Ed.* **2001**, *40*, 2427.

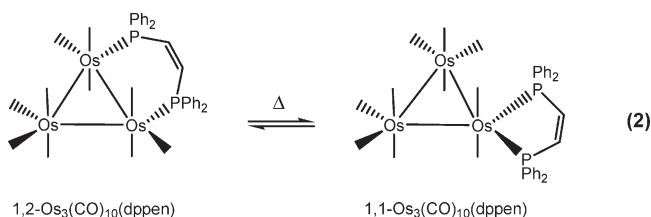
(7) Balch, A. L.; Davis, B. J.; Olmstead, M. M. *J. Am. Chem. Soc.* **1990**, *112*, 8592. *Inorg. Chem.* **1993**, *32*, 3937.

(8) (a) Hoffmann, R. *Angew. Chem., Int. Ed.* **1982**, *21*, 711. (b) Mingos, D. M. P.; Wales, D. J. *Introduction to Cluster Chemistry*; Prentice Hall: Englewood Cliffs, NJ, 1990.

(9) (a) Pechmann, T.; Brandt, C. D.; Werner, H. *Angew. Chem., Int. Ed.* **2000**, *39*, 3909. (b) Pechmann, T.; Brandt, C. D.; Roger, C.; Werner, H. *Angew. Chem., Int. Ed.* **2002**, *41*, 2301. (c) Pechmann, T.; Brandt, C. D.; Werner, H. *Dalton Trans.* **2004**, 959. (d) Pechmann, T.; Brandt, C. D.; Werner, H. *Chem. Eur. J.* **2004**, *10*, 728.

(10) (a) Sauthier, M.; Le Guennic, B.; Deborde, V.; Toupet, L.; Halet, J.-F.; Réau, R. *Angew. Chem., Int. Ed.* **2001**, *40*, 228. (b) Leca, F.; Sauthier, M.; Deborde, V.; Toupet, L.; Réau, R. *Chem. Eur. J.* **2003**, *9*, 3785. (c) Leca, F.; Lescop, C.; Rodriguez-Sanz, E.; Costuas, K.; Halet, J.-F.; Réau, R. *Angew. Chem., Int. Ed.* **2005**, *44*, 4362. (d) Nohra, B.; Rodriguez-Sanz, E.; Lescop, C.; Réau, R. *Chem. Eur. J.* **2008**, *14*, 3391.

One of us (M.G.R.) has held a long-term interest in the synthesis and mechanistic study of Ru_3 , Os_3 , and tetrahedrane clusters, containing rigid diphosphine ligands.^{15c,20–22} Several of these reports have addressed the dynamic isomerization of the ancillary diphosphine ligand about the cluster core, as illustrated for the cluster compound $\text{Os}_3(\text{CO})_{10}(\text{dppen})$ (where $\text{dppen} = (\text{Z})\text{-}1,2\text{-bis}(\text{diphenylphosphino})\text{-ethylene}$) in eq 2. This particular reaction is reversible, and the thermodynamically favored isomer contains a chelating dppen ligand with a K_{eq} value of 6.9 over the temperature range 358–373 K.^{21a} The dppen isomerization, from bridging to chelating, is unaffected by added CO, and the activation parameters for the forward and reverse reactions indicate an ordered transition state. The reaction kinetics are consistent with a nondissociative scenario for this rearrangement, requiring, at a minimum, the formal site exchange of at least one phosphine and one CO across an Os–Os bond, presumably by way of a transient $\mu_2\text{-phosphine}/\mu_2\text{-CO}$ species.



In order to establish the influence that the differences between closely related diphosphine ligands have on the reactivity of the isomeric $\text{Os}_3(\text{CO})_{10}(\text{P-P})$ clusters, we have investigated the reaction of 1,2-bis(diphenylphosphino)benzene (dppbz) and 1,2-bis(diphenylphosphino)tetrafluorobenzene (dppbzF_4) with the trismium cluster $1,2\text{-Os}_3(\text{CO})_{10}(\text{MeCN})_2$ (**1**). The dppbz ligand reacts with $1,2\text{-Os}_3(\text{CO})_{10}(\text{MeCN})_2$ to furnish bridged $1,2\text{-Os}_3(\text{CO})_{10}(\text{dppbz})$ as the kinetic product of ligand substitution, and the kinetics for isomerization to the corresponding chelated isomer, $1,1\text{-Os}_3(\text{CO})_{10}(\text{dppbz})$, have been followed by UV–vis spectroscopy. In contrast to the reaction of **1** with dppbz , the reaction between **1** and dppbzF_4 affords chelated $1,1\text{-Os}_3(\text{CO})_{10}(\text{dppbzF}_4)$ as the sole observable product. Presumably, the bridged isomer is again formed but rearranges rapidly to the chelated isomer.

We have performed DFT calculations, in order to explore the effect that different diphosphine ligands have on the thermodynamic and kinetic stabilities of the bridged and chelated isomers in the $\text{Os}_3(\text{CO})_{10}(\text{P-P})$ clusters. In the course of establishing the mechanism for the rearrangement

(19) Jesson, J. P.; Muetterties, E. L. In *Dynamic Nuclear Magnetic Resonance Spectroscopy*; Jackman, L. M., Cotton, F. A., Eds.; Academic Press: New York, 1975; Chapter 8.

(20) For Ru_3 clusters: (a) Shen, H.; Bott, S. G.; Richmond, M. G. *Organometallics* **1995**, *14*, 4625. (b) Bott, S. G.; Shen, H.; Senter, R. A.; Richmond, M. G. *Organometallics* **2003**, *22*, 1953. (c) Bott, S. G.; Shen, H.; Richmond, M. G. *J. Organomet. Chem.* **2004**, *689*, 3426. **2005**, *690*, 3838. (d) Bott, S. G.; Shen, H.; Huang, S.-H.; Richmond, M. G. *J. Organomet. Chem.* **2008**, *693*, 2327.

(21) For Os_3 clusters: (a) Watson, W. H.; Wu, G.; Richmond, M. G. *Organometallics* **2005**, *24*, 5431. (b) Watson, W. H.; Wu, G.; Richmond, M. G. *Organometallics* **2006**, *25*, 930. (c) Watson, W. H.; Poola, B.; Richmond, M. G. *J. Organomet. Chem.* **2006**, *691*, 4676. (d) Watson, W. H.; Poola, B.; Richmond, M. G. *Polyhedron* **2007**, *26*, 3585.

(22) For tetrahedrane clusters: (a) Bott, S. G.; Yang, K.; Talafuse, K. A.; Richmond, M. G. *Organometallics* **2003**, *22*, 1383. (b) Bott, S. G.; Yang, K.; Richmond, M. G. *J. Organomet. Chem.* **2005**, *690*, 3067; **2006**, *691*, 3771 (c) Watson, W. H.; Bodige, S. G.; Ejsmont, K.; Liu, J.; Richmond, M. G. *J. Organomet. Chem.* **2006**, *691*, 3609.

of bridged to chelated isomers, we investigated the nature of the preferred pathway that is responsible for nondissociative ligand isomerization in this genre of clusters.

Experimental Section

General Methods. The parent cluster $\text{Os}_3(\text{CO})_{12}$ was prepared from OsO_4 and CO,²³ and this cluster was used in the preparation of the bis(acetonitrile) cluster $1,2\text{-Os}_3(\text{CO})_{10}(\text{MeCN})_2$.²⁴ The dppbzF_4 ligand was synthesized from 1,2-dibromotetrafluorobenzene and Ph_2PCl according to the procedure of Meek.²⁵ The OsO_4 used in our studies was purchased from Engelhard Chemical Co., and the chemicals $\text{Me}_3\text{NO}\cdot x\text{H}_2\text{O}$, dppbz , 1,2-dibromotetrafluorobenzene, chlorodiphenylphosphine, and BuLi (2.5 M in hexanes) were purchased from Aldrich Chemical Co. The anhydrous Me_3NO employed in our studies was obtained from $\text{Me}_3\text{NO}\cdot x\text{H}_2\text{O}$, after the waters of hydration were azeotropically removed under reflux, using benzene as a solvent. All reaction solvents were distilled from a suitable drying agent under argon or obtained from an Innovative Technology (IT) solvent purification system. When not in use, all purified solvents were stored in Schlenk storage vessels equipped with high-vacuum Teflon stopcocks.²⁶ The NMR solvents CDCl_3 and C_6D_6 were purified by bulb-to-bulb distillation from P_2O_5 and sodium/benzophenone ketyl, respectively. Combustion analyses were performed by Atlantic Microlab, Norcross, GA.

The IR spectra were recorded on a Nicolet 6700 FT-IR spectrometer in amalgamated NaCl cells having a 0.1 mm path length, while the quoted ^1H NMR data were recorded at 400 and 500 MHz on Varian VXR-400 and VXR-500 spectrometers, respectively. The ^{31}P NMR spectra were recorded at 202 MHz on the latter spectrometer. These data were collected in the proton-decoupled mode and are referenced to external H_3PO_4 (85%), whose chemical shift was set at δ 0.

Preparation of $1,2\text{-Os}_3(\text{CO})_{10}(\text{dppbz})$ from $1,2\text{-Os}_3(\text{CO})_{10}(\text{MeCN})_2$ and dppbz . To 0.25 g (0.27 mmol) of $1,2\text{-Os}_3(\text{CO})_{10}(\text{MeCN})_2$ in a Schlenk tube was added 0.14 g (0.31 mmol) of dppbz , followed by 30 mL of CH_2Cl_2 via syringe. The solution was stirred for 3 h at room temperature and then examined by TLC analysis (1/1 CH_2Cl_2 /hexane), which revealed the consumption of the starting cluster, a trace amount of unreacted dppbz ($R_f = 0.53$), and a yellow spot ($R_f = 0.48$) corresponding primarily to **2** (78%), along with minor amounts of **3** (20%) and **4** (ca. 2%), whose presence was established by NMR spectroscopy. The ternary cluster mixture, composed of **2–4**, could not be separated into individual components; these products were isolated as a mixture by flash-column chromatography over alumina at 0 °C, using the aforementioned eluent. Spectroscopic data for cluster **2**²⁷ are as follows. IR (CH_2Cl_2): $\nu(\text{CO})$ 2092 (s), 2041 (m), 2013 (s), 2004 (m), 1973 (cm^{-1}). ^1H NMR (CDCl_3): δ 6.78–7.50 (m, aryl). ^{31}P NMR (CDCl_3): δ 6.41 (s).

Isomerization of $1,2\text{-Os}_3(\text{CO})_{10}(\text{dppbz})$ to $1,1\text{-Os}_3(\text{CO})_{10}(\text{dppbz})$ under CO. The above cluster mixture (ca. 0.33 g) was heated in toluene at 60 °C under 1 atm of CO for 24 h, after which time ^{31}P NMR analysis of the solution revealed the presence of only cluster **3**. The solvent was removed under vacuum and the residue chromatographed over alumina using a 1/1 CH_2Cl_2 /hexane mixture. The crude product was recrystallized from CH_2Cl_2 and hexane at 5 °C to afford **3** as a dark yellow solid. Yield: 0.31 g (94%). IR (CH_2Cl_2): $\nu(\text{CO})$ 2094 (s),

(23) Drake, S. R.; Loveday, P. A. *Inorg. Synth.* **1990**, *28*, 230.

(24) Nicholls, J. N.; Vargas, M. D. *Inorg. Synth.* **1989**, *26*, 289.

(25) Eller, P. G.; Meek, D. W. *J. Organomet. Chem.* **1970**, *22*, 631.

(26) Shriver, D. F. *The Manipulation of Air-Sensitive Compounds*; McGraw-Hill: New York, 1969.

(27) A relatively pure IR spectrum of cluster **2** was obtained after suitable spectral subtraction of clusters **3** and **4** from the initial ternary cluster mixture.

Table 1. X-ray Crystallographic Data and Processing Parameters for the dppbz-Substituted Clusters **2**·CH₂Cl₂, **3**, and **4**·CH₂Cl₂

	2 ·CH ₂ Cl ₂	3	4 ·CH ₂ Cl ₂
CCDC entry no.	770699	770697	770702
cryst syst	triclinic	monoclinic	orthorhombic
space group	$P\bar{1}$	$P2_1/c$	$Pbca$
<i>a</i> , Å	11.9406(3)	10.983(2)	21.745(2)
<i>b</i> , Å	13.2173(4)	20.218(3)	16.774(2)
<i>c</i> , Å	15.0648(4)	17.530(3)	21.934(2)
α , deg	86.091(1)		
β , deg	70.006(1)	96.856(3)	
γ , deg	66.423(1)		
<i>V</i> , Å ³	2041.2(1)	3865(1)	8001(1)
mol formula	C ₄₁ H ₂₆ Cl ₂ O ₁₀ Os ₃ P ₂	C ₄₀ H ₂₄ O ₁₀ Os ₃ P ₂	C ₄₀ H ₂₆ Cl ₂ O ₉ Os ₃ P ₂
fw	1382.06	1297.13	1354.05
formula units per cell (Z)	2	4	8
<i>D</i> _{calcd} , Mg/m ³	2.249	2.229	2.248
λ (Mo K α), Å	0.710 73	0.710 73	0.710 73
μ , mm ⁻¹	9.581	9.979	9.773
abs cor	semiempirical from equivalents	empirical from equivalents	semiempirical
<i>F</i> (000)	1288	2408	5040
cryst size, mm	0.11 × 0.08 × 0.06	0.28 × 0.14 × 0.03	0.24 × 0.17 × 0.06
abs cor factor	0.5971/0.4188	0.9942/0.3008	0.5917/0.2026
total no. of rflns	24 301	32 839	14 706
no. of indep rflns	8375	9099	14 832
no. of data/residuals/params	8375/0/523	9099/0/496	14 832/4/516
R1 ^a (<i>I</i> ≥ 2 σ (<i>I</i>))	0.0140	0.0301	0.0388
wR2 ^b	0.0322	0.0492	0.0697
GOF on <i>F</i> ²	1.012	0.905	1.028
max, min $\Delta\rho$, e/Å ³	1.114, -0.402	0.902, -1.218	2.434, -2.301

$$^a R1 = \sum ||F_o| - |F_c|| / \sum |F_o|. \quad ^b wR2 = \{ \sum [w(F_o^2 - F_c^2)]^2 / \sum [w(F_o^2)]^2 \}^{1/2}.$$

2040 (m), 2011 (s), 2001 (m), 1971 (w) cm⁻¹. ¹H NMR (C₆D₆): δ 6.78 (unresolved multiplet, 2H, aryl platform), 6.94 (t, 4H, para, aryl, $J_{H-H} = 7.3$ Hz), 7.04 (t, 8H, meta, aryl, $J_{H-H} = 7.3$ Hz), 7.30 (unresolved multiplet, 2H, aryl platform), 7.49 (bm, 8H, ortho, aryl). ³¹P NMR (C₆D₆): δ 26.32 (s). Anal. Calcd (found) for C₄₀H₂₄O₁₀Os₃P₂·^{1/2}CH₂Cl₂: C, 36.31 (36.19); H, 1.88 (1.75).

Photolysis of 1,1-Os₃(CO)₁₀(dppbz) To Give HO₃(CO)₉[μ -1,2-PhP(C₆H₄- η ¹)C₆H₄PPh₂]. A small Schlenk tube was charged with 0.10 g (0.077 mmol) of **3** and 25 mL of toluene, after which the vessel was sealed and subjected to three freeze-pump-thaw degas cycles. The vessel was then irradiated (366 nm) at room temperature for a period of 5 days. The CO that accompanies the formation of **4** was periodically removed by additional freeze-pump-thaw degas cycles, in order to drive the reaction to completion. At the end of the photolysis, the solution was concentrated under vacuum; the residue was passed over a short pad of alumina, using 1/1 CH₂Cl₂/hexane as the eluent, to furnish a yellow solid. Recrystallization of **4** from CH₂Cl₂/benzene afforded the desired product in 88% yield (86 mg). IR (CH₂Cl₂): ν (CO) 2075 (s), 2038 (vs), 2013 (s), 1997 (s), 1967 (m) cm⁻¹. ¹H NMR (C₆D₆): δ -16.43 (dd, hydride, $J_{P-H} = 12.5$ and 16.0 Hz), 6.68–7.52 (m, 22H, aryl), 8.36 (dd, 1H, metalated aryl, $J_{H-H} = 2.5$ and 6.5 Hz). ³¹P NMR (C₆D₆): δ 28.62 (d, $J_{P-P} = 13.3$ Hz), 39.54 (d, $J_{P-P} = 13.3$ Hz). Anal. Calcd (found) for C₄₀H₂₄O₁₀Os₃P₂·^{1/2}C₆H₆: C, 38.53 (38.15); H, 2.06 (2.50).

Reaction of 1,2-Os₃(CO)₁₀(MeCN)₂ with dppbzF₄ To Give 1,1-Os₃(CO)₁₀(dppbzF₄). To 0.20 g (0.21 mmol) of 1,2-Os₃(CO)₁₀(MeCN)₂ in 50 mL of benzene was added 0.12 g (0.23 mmol) of dppbzF₄ under argon flush. The solution was stirred at room temperature and monitored by TLC, which confirmed the consumption of the starting cluster and the presence of a yellow spot ascribed to cluster **6** ($R_f = 0.79$ in 1/1 CH₂Cl₂/hexane) after ca. 1 h. The solvent was removed under vacuum and the desired product purified by chromatography over silica gel employing 1/1 CH₂Cl₂/hexane as the mobile phase. The isolated product was recrystallized from CH₂Cl₂/hexane at 5 °C to furnish 0.25 g (85%) of analytically pure **6**. IR (CH₂Cl₂): ν (CO) 2095 (s), 2046 (s), 2010 (vs), 1992 (m), 1975 (m), 1962 (m), 1927 (w) cm⁻¹. ¹H NMR (C₆D₆): δ 7.20 (t, 4H, para, $J_{H-H} = 8.0$ Hz), 7.34 (dt, 8H,

meta, $J_{H-H} = 8.0$ Hz, $J_{P-H} = 2.7$ Hz), 7.76 (dd, 8H, ortho, $J_{P-H} = 11.5$ Hz, $J_{H-H} = 8.0$ Hz). ³¹P NMR (CDCl₃): δ 34.00 (s). Anal. Calcd (found) for C₄₀H₂₀F₄O₁₀Os₃P₂: C, 35.09 (34.82); H, 1.47 (1.56).

Photolysis of 1,1-Os₃(CO)₁₀(dppbzF₄) To Give HO₃(CO)₉[μ -1,2-PhP(C₆H₄- η ¹)C₆F₄PPh₂]. A 50 mg (0.037 mmol) portion of **6** was charged to a NMR tube equipped with a J. Young valve, followed by 0.7 mL of C₆D₆. The solution was evacuated via two freeze-pump-thaw degas cycles, and the NMR tube was irradiated at 366 nm at room temperature for a period of 24 h. The liberated CO was removed by three periodic freeze-pump-thaw cycles during the course of the reaction. Once the NMR analysis confirmed the disappearance of **6**, the irradiation was terminated and the solvent removed. The desired product was subsequently isolated by column chromatography over silica gel using 1/1 CH₂Cl₂/hexane, after which the product was recrystallized from hexane/benzene to afford **7** in 90% yield (44 mg). IR (CH₂Cl₂): ν (CO) 2085 (s), 2025 (s), 2002 (vs), 1996 (m), 1951 (m) cm⁻¹. ¹H NMR (C₆D₆): δ -16.13 (dd, hydride, $J_{P-H} = 13.8$ and 14.2 Hz), 6.88 (bm, 2H, metalated aryl), 6.97–7.16 (m, 10H), 7.56 (m, 3H), 7.68 (m, 2H), 8.05 (bt, 1H, metalated aryl, $J_{H-H} = 7.5$ Hz), 8.37 (m, 1H, metalated aryl). ²⁸³¹P NMR (CDCl₃): δ 41.17 (b, unresolved fluorine coupling), 44.43 (b, unresolved fluorine coupling). Anal. Calcd (found) for C₃₉H₂₀F₄O₉Os₃P₂·^{1/2}C₆H₆: C, 36.52 (37.01); H, 1.67 (2.18).

Isomerization Kinetics. The conversion **2** → **3** was investigated by UV-vis spectroscopy in quartz UV-visible cells (1.0 cm width) that were equipped with a high-vacuum Teflon stopcock, to facilitate handling on the vacuum line. Samples of **2** in toluene solution were purged with CO at room temperature immediately before the start of each kinetic experiment, in order to suppress the formation of the hydride cluster **4**. The experiments conducted at 6.8 and 34 atm of CO were carried out in a carbon-steel 300 mL autoclave, where the reaction pressure was controlled by a Tescom pressure regulator. The autoclave was equipped with a tip tube that enabled sample removal for UV-vis analysis while maintaining constant CO pressure. The Hewlett-Packard 8452A

(28) The quoted J_{P-H} values for the bridging hydride were determined by spectral simulation using the program gNMR.

Table 2. X-ray Crystallographic Data and Processing Parameters for the dppbzF_4 -Substituted Clusters $6 \cdot 1/2\text{C}_6\text{H}_6$ and $7 \cdot \text{CHCl}_3$

	$6 \cdot 1/2\text{C}_6\text{H}_6$	$7 \cdot \text{CHCl}_3$
CCDC entry no.	770698	770701
cryst syst	triclinic	monoclinic
space group	$P\bar{1}$	$P2_1/n$
a , Å	12.1322(5)	11.4132(6)
b , Å	17.5733(8)	19.109(1)
c , Å	21.598(1)	18.870(1)
α , deg	94.371(1)	
β , deg	101.218(1)	95.543(1)
γ , deg	106.671(1)	
V , Å ³	4284.0(3)	4096.0(4)
mol formula	$\text{C}_{43}\text{H}_{23}\text{F}_4\text{O}_{10}\text{Os}_3\text{P}_2$	$\text{C}_{40}\text{H}_{20}\text{Cl}_3\text{F}_4\text{O}_9\text{Os}_3\text{P}_2$
fw	1408.15	1459.45
formula units per cell (Z)	4	4
D_{calcd} , Mg/m ³	2.183	2.367
$\lambda(\text{Mo K}\alpha)$, Å	0.710 73	0.710 73
μ , mm ⁻¹	9.025	9.631
abs cor	semiempirical from equivalents	semiempirical from equivalents
$F(000)$	2620	2708
cryst size, mm	$0.27 \times 0.26 \times 0.06$	$0.23 \times 0.11 \times 0.07$
abs cor factor	0.6055/0.1927	0.5096/0.2371
total no. of rflns	53 669	48 738
no. of indep rflns	18 867	8685
no. of data/residuals/params	18 867/187/1128	8685/0/547
$R1^a$ ($I \geq 2\sigma(I)$)	0.0240	0.0238
$wR2^b$	0.0287	0.0300
GOF on F^2	1.026	1.041
max, min $\Delta\rho$, e/Å ³	1.779, -1.696	3.353, -1.123

$$^a R1 = \sum ||F_o| - |F_c|| / \sum |F_o|. \quad ^b wR2 = \{ \sum [w(F_o^2 - F_c^2)]^2 / \sum [w(F_o^2)] \}^{1/2}.$$

diode array spectrometer employed in our studies was configured with a custom VT cell holder, which was connected to a Neslab RTE7 constant-temperature circulator. The quoted reaction temperatures are considered to be accurate to within ± 0.5 K. The progress of the isomerization reactions, conducted at 1 atm of CO, was monitored by following the optical changes of the 365 nm band as a function of time for at least 4–6 half-lives, while those reactions carried out under higher CO pressure were examined out to 3 half-lives. The UV–vis derived rate constants, quoted in Table 3, were determined by nonlinear regression analysis, using a single-exponential function, with the initial (A_0) and final (A_∞) absorbance values and the rate constant (k) treated as free variables in the calculation.²⁹ The activation parameters for the isomerization $2 \rightarrow 3$ were calculated from a plot of $\ln(k/T)$ versus T^{-1} ,³⁰ with the error limits representing the deviation of the data points about the least-squares line of the Eyring plot.

X-ray Diffraction Data for Clusters 2–6. Single crystals of the cluster compounds **2–4**, suitable for X-ray diffraction analyses, were grown from CH_2Cl_2 and hexane, while X-ray-quality crystals of **6** and **7** were grown from benzene/hexane and CHCl_3 /hexane, respectively. With the exception of cluster **3**, whose X-ray data were collected at TCU on a Bruker SMART 1000 CCD-based diffractometer at 213(2) K, all of the other structures were collected at UNT on a Bruker X8 APEX CCD diffractometer at 100(2) K. The frames were integrated with the available SAINT³¹ (TCU) and APEX2³² (UNT) software packages, using a narrow-frame algorithm; the structures were solved and refined using the SHELXTL program package.³³

The molecular structures were checked using PLATON,³⁴ and the non-hydrogen atoms were refined anisotropically, except where otherwise noted. All hydrogen atoms were assigned calculated positions and allowed to ride on the attached carbon atom. The cluster $4 \cdot \text{CH}_2\text{Cl}_2$ was found to be twinned in the first domain by 178.1° about the reciprocal axis $-0.010, 1.000, 0.008$ (twin ratio 0.625:0.375). The structure was refined using unmerged data in HKL5 format and contained a disordered solvent. These drawbacks affected the quality of the collected X-ray data and prevented the accurate location of the bridging hydride group that is assumed to span the Os(2)–Os(3) vector in $4 \cdot \text{CH}_2\text{Cl}_2$. The cluster $6 \cdot 1/2\text{C}_6\text{H}_6$ exists as two independent 1,1-Os₃(CO)₁₀(dppbzF₄) molecules in the asymmetric unit of the triclinic cell ($Z' = 2$). Disorder was found for the phenyl groups on the atoms P2 and P3 and the benzene solvent molecules located on inversion centers 1f and 1e. The disordered parts were refined accordingly with distance restraints to simulate the hexagonal shape of the aromatic rings. Tables 1 and 2 summarize the pertinent X-ray data and processing parameters for these trismium clusters.

Computational Methodology. All calculations were performed with the Gaussian 03 package of programs.³⁵ The calculations were carried out with the B3LYP functional, which is comprised of Becke's linear combination of three functionals³⁶ and the correlation functional of Lee, Yang, and Parr.³⁷ The Os atoms were described by Stuttgart–Dresden effective core potentials and the SDD basis set.³⁸ The D95* basis set was used for the P, O, C, and H atoms.³⁹

(29) The rate calculations were performed by using the equation $A(t) = A_\infty + \Delta A e^{-kt}$ with the aid of the commercially available program Origin6.0.

(30) Carpenter, B. K. *Determination of Organic Reaction Mechanisms*; Wiley-Interscience: New York, 1984.

(31) *Saint Version 6.02*; Bruker Advanced Analytical X-ray Systems, Inc., 1997–1999.

(32) *APEX2 Version 2.14*; Bruker Advanced Analytical X-ray Systems, Inc., Madison, WI, 2007.

(33) *SHELXTL Version 5.1*; Bruker Advanced Analytical X-ray Systems, Inc., Madison, WI, 1998.

(34) Spek, A. L. *J. Appl. Crystallogr.* **2003**, *36*, 7.

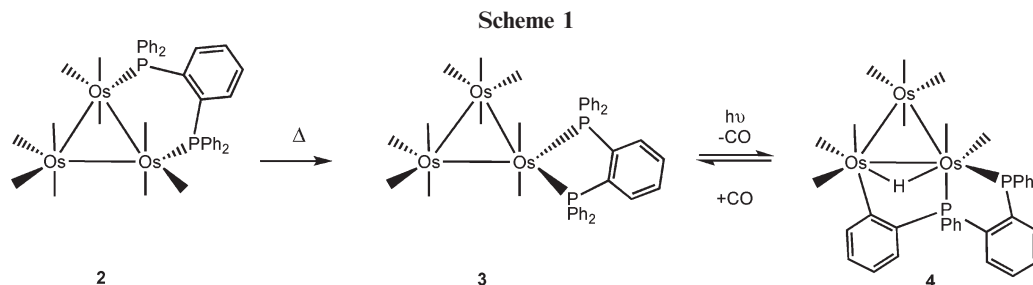
(35) Frisch, M. J. et al. *Gaussian 03, Revision E.01*; Gaussian, Inc., Pittsburgh, PA, 2003.

(36) Becke, A. D. *Phys. Rev. A* **1988**, *38*, 3098.

(37) (a) Lee, C.; Yang, W.; Parr, R. G. *Phys. Rev. B* **1988**, *37*, 785. (b) Miehlich, B.; Savin, A.; Stoll, H.; Preuss, H. *Chem. Phys. Lett.* **1989**, *157*, 200.

(38) Dolg, M. In *Modern Methods and Algorithms of Quantum Chemistry*; Grotendorst, J., Ed.; John von Neumann Institute for Computing: Jülich, 2000; Vol. 1, p 479.

(39) Dunning, T. H., Jr.; Hay, P. J. In *Modern Theoretical Chemistry*; Schaefer, H. F., III, Ed.; Plenum: New York, 1976; Vol. 3, pp 1–28.



Geometries were fully optimized, and analytical second derivatives were evaluated at each stationary point, to establish whether the geometry was an energy minimum (no imaginary frequencies) or a transition structure (one imaginary frequency). The computed frequencies were used to make zero-point and thermal corrections to the electronic energies.

Results and Discussion

I. Diphosphine Bridging and Chelation in the Reaction of 1,2-Os₃(CO)₁₀(MeCN)₂ with dppbz. The labile cluster 1,2-Os₃(CO)₁₀(MeCN)₂ reacts rapidly with the diphosphine ligand dppbz at room temperature, to furnish the corresponding diphosphine-bridged cluster 1,2-Os₃(CO)₁₀(dppbz) (**2**) as the major product. The yield of crude product was 78%, as assessed by ³¹P NMR analysis of an aliquot of the reaction mixture before purification.⁴⁰ Accompanying **2** in the reaction mixture were the isomeric chelated cluster 1,1-Os₃(CO)₁₀(dppbz) (**3**) and the hydride cluster HOs₃(CO)₉[μ-1,2-PhP(C₆H₄-η¹C₆H₄PPh₂)] (**4**), which were formed in 20% and 2% yields, respectively. These two minor products both result from the isomerization of **2** to **3**. Decarbonylation of the latter cluster leads to ortho metalation and the formation of **4** (vide infra). The relationship between these dppbz-substituted clusters is summarized in Scheme 1.

TLC analysis of the crude reaction mixture revealed the presence of only one spot for the three products; therefore, the ternary mixture was isolated by flash-column chromatography and characterized in solution as an aggregate. The spectroscopic properties of **2** are consistent with its formulated structure. The bridging dppbz appears as a singlet in the ³¹P NMR spectrum at δ 6.41. The different aromatic hydrogens, associated with the four phenyl groups (Ph) and the benzo group, could not be assigned with certainty due to extensive overlap.

The thermal ellipsoid plot of the molecular structure of **2**, as the CH₂Cl₂ solvate, shown in Figure 1 confirms the bridging disposition of the dppbz ligand, which spans the Os(1)–Os(2) vector. The Os–Os bond distances range from 2.8507(1) Å (Os(1)–Os(2)) to 2.8821(1) Å (Os(2)–Os(3)), and the Os(1)–P(1) and Os(2)–P(2) bond distances of 2.3359(6) and 2.3289(6) Å are slightly longer than those distances reported by us for 1,2-Os₃(CO)₁₀(dppen) but are well within the accepted range observed in a variety of

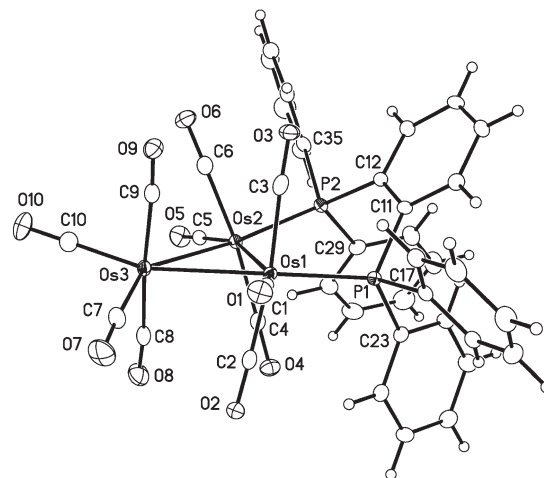


Figure 1. Thermal ellipsoid plot of **2**·CH₂Cl₂ at the 50% probability level with the hydrogen atoms shown as small spheres of arbitrary radii. The CH₂Cl₂ solvent has been omitted for clarity. Selected bond distances (Å) and angles (deg): Os(1)–P(1) = 2.3359(6), Os(1)–Os(2) = 2.8507(1), Os(1)–Os(2) = 2.8547(1), Os(2)–P(2) = 2.3289(6), Os(2)–Os(3) = 2.8821(1), P(1)···P(2) = 3.6073(9); P(1)–Os(1)–Os(3) = 155.39(2), P(2)–Os(2)–Os(3) = 156.27(2), C(11)–P(1)–Os(1) = 114.73(8), C(12)–P(2)–Os(2) = 120.62(8), C(12)–C(11)–P(1) = 125.3(2), C(11)–C(12)–P(2) = 126.6(2).

phosphine-substituted polynuclear compounds.^{21a,41} While the P(1) and P(2) atoms are equatorially disposed, they are tipped out of the plane defined by the three osmium atoms by 0.2765(6) and –0.5657(6) Å, respectively. The *o*-phenylene platform that serves to tether the vicinal Ph₂P moieties is defined by the atoms C(11)–C(16), and this group is also tipped out of the metallic plane with a fold angle of 48.89(3)°. The ancillary carbonyl ligands are best viewed as linear groups, and the axial CO groups exhibit the commonly observed *D*₃ twist with respect to the metallic core.⁴²

The bridging of the Os(1) and Os(2) atoms by the dppbz ligand in **2** is thermodynamically less favorable than the chelation in isomer **3**. This factor also serves as the driving force for the facile isomerizations, observed in related, diphosphine-bridged isomers of Os₃(CO)₁₀(P-P).²¹ Three significantly adverse perturbations result from the stretching of the dppbz ligand across the Os(1)–Os(2) vector in **2**, and they in turn account for the ground-state destabilization in **2** relative to **3**. The bridging dppbz ligand in **2** exhibits a

(40) Phosphine ligand substitution in 1,2-Os₃(CO)₁₀(MeCN)₂ has been previously shown by Poë to proceed through a dissociative loss of the MeCN ligands. In the present case, capture of the initial unsaturated cluster, Os₃(CO)₁₀(MeCN), by the dppbz is predicted to afford Os₃(CO)₁₀(MeCN)(η¹-dppbz) with a pendant phosphine ligand. Rapid ring closure to generate **2** is the anticipated result from either MeCN dissociation or an associative interchange process where MeCN serves as the leaving group. See: (a) Dahlinger, K.; Poë, A. J.; Sayal, P. K.; Sekhar, V. C. *Dalton Trans.* **1986**, 2145. (b) Hudson, R. H. E.; Poë, A. J.; Sampson, C. N.; Siegel, A. *Dalton Trans.* **1989**, 2235.

(41) Orpen, A. G.; Brammer, L.; Allen, F. K.; Kennard, O.; Watson, D. G.; Taylor, R. *Dalton Trans.* **1989**, S1.

(42) (a) Alex, R. F.; Einstein, F. W. B.; Jones, R. H.; Pomeroy, R. K. *Inorg. Chem.* **1987**, *26*, 3175. (b) Bruce, M. I.; Liddell, M. J.; Skawkataly, O. B.; Hughes, C. A.; Skelton, B. H.; White, A. H. *J. Organomet. Chem.* **1988**, *347*, 207.

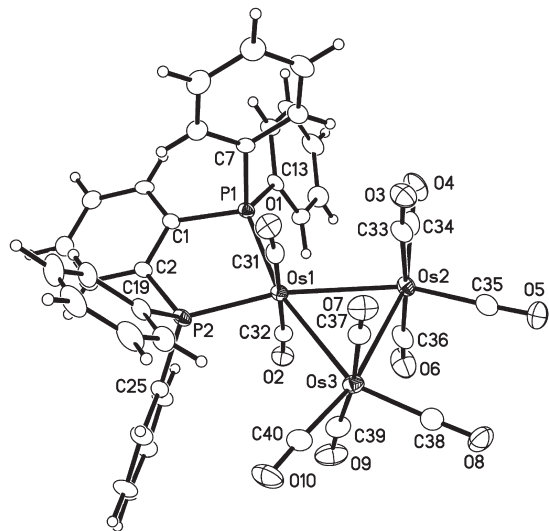


Figure 2. Thermal ellipsoid plot of **3** at the 30% probability level with the hydrogen atoms shown as small spheres of arbitrary radii. Selected bond distances (Å) and angles (deg): Os(1)–P(2) = 2.290(1), Os(1)–P(1) = 2.294(1), Os(1)–Os(2) = 2.9092(5), Os(1)–Os(3) = 2.9263(5), Os(2)–Os(3) = 2.9109(4), P(1)···P(2) = 3.094(2); P(2)–Os(1)–P(1) = 84.90(4), P(2)–Os(1)–Os(2) = 168.58(3), P(1)–Os(1)–Os(2) = 164.46(3), C(1)–P(1)–Os(1) = 108.6(2), C(2)–P(2)–Os(1) = 108.6(2), C(2)–C(1)–P(1) = 116.9(3), C(1)–C(2)–P(2) = 117.9(3).

P(1)···P(2) internuclear bond distance (3.6073(9) Å) that is >0.4 Å longer than the P(1)···P(2) internuclear bond distance reported for the free dppbz ligand.⁴³ The angular deviation from sp^2 hybridization of the *o*-phenylene C(11) and C(12) carbons found in the C(12)–C(11)–P(1) (125.3(2)°) and C(11)–C(12)–P(2) (126.6(2)°) linkages exceeds the accepted VSEPR angle of 120° by >5°. A similar deformation from the accepted sp^3 hybridization bond angle of ca. 109° is also evidenced in the angles of 114.73(8) and 120.62(8)° for the C(11)–P(1)–Os(1) and C(12)–P(2)–Os(2) linkages, respectively. The observed fold angle of 43.95(2)° along the P(1)···P(2) hinge of the six-membered ring, defined by the $Os_2P_2C_2$ atoms, underscores the non-planar disposition that exists between the *o*-phenylene and Os_3 rings in **2**.

Heating the ternary mixture of **2**–**4** under 1 atm of CO at 333 K overnight afforded **3** as the sole observable product, as determined by ¹H and ³¹P NMR spectroscopy. This transformation verifies that **3** is the thermodynamically most stable of the isomeric $Os_3(CO)_{10}(dppbz)$ clusters. The addition of CO suppresses the formation of the hydride cluster **4**, but CO addition has been shown not to affect the equilibrium for the bridged-to-chelated ligand isomerization in other decacarbonyl clusters $Os_3(CO)_{10}(P-P)$.²¹

Cluster **3** was isolated by column chromatography and characterized in solution by IR and NMR spectroscopy; the molecular structure was determined by X-ray diffraction analysis. The singlet recorded at δ 26.32 in the ³¹P NMR spectrum of **3** is in full agreement with a triosmium cluster possessing a chelating dppbz ligand. Figure 2 shows the thermal ellipsoid plot of the molecular structure of **3** and confirms the attendant isomerization of the dppbz ligand upon heating. The Os–Os bond distances range from

(43) Levason, W.; Reid, G.; Webster, M. *Acta Crystallogr.* **2006**, C62, 440.

Table 3. Experimental Rate Constants for the Isomerization of 1,2- $Os_3(CO)_{10}(dppbz)$ to 1,1- $Os_3(CO)_{10}(dppbz)$ under CO^a

entry	temp (K)	10^4k (s ⁻¹)
1	318.0	0.29(8)
2	323.0	0.50(7)
3	323.0	0.45(10) ^b
4	323.0	0.58(9) ^c
5	323.0	0.49(8) ^d
6	328.0	1.01(12)
7	333.0	1.41(10)
8	338.0	2.63(16)
9	343.0	3.66(14)

^aThe UV–vis kinetic data were collected in toluene using a ca. 10^{-4} M solution of starting cluster by following the increase in the absorbance of the 365 nm band. Unless otherwise noted, all reactions were performed under 1 atm of CO. ^bReaction carried out in an autoclave under 6.8 atm of CO. ^cReaction carried out in an autoclave under 34 atm of CO. ^dReaction carried out under argon in the presence of 10 equiv of PPh₃.

2.9092(5) Å (Os(1)–Os(2)) to 2.9263(5) Å (Os(1)–Os(3)). The internuclear P(1)···P(2) distance of 3.094(2) Å has undergone a significant contraction, relative to that distance found in **2**, and the angles associated with the Os(1)–P(1)–C(1) (108.6(2)°), Os(1)–P(2)–C(2) (108.6(2)°), C(2)–C(1)–P(1) (116.9(3)°), and C(1)–C(2)–P(2) (117.9(3)°) linkages display values that are in excellent agreement with the idealized hybridization state of the subtended atom. The observed angle of 84.90(4)° for the P(1)–Os(1)–P(2) atoms is in keeping with the chelating nature of the ancillary dppbz ligand and the bite angle reported in the three known dppbz-chelated clusters $Ir_4(CO)_{10}(dppbz)$,⁴⁴ $H_4Ru_4(CO)_{10}(dppbz)$,⁴⁵ and $HRu_6(\mu_5-C)(\mu_3-P)(CO)_{14}(dppbz)$.⁴⁶ The remaining bond distances and angles are unremarkable and require no comment.

Our interest in the coordinative flexibility of diphosphine ligands in polynuclear clusters^{21,22} led us to measure the kinetics for the conversion **2** → **3**. The isomerization reactions were conveniently monitored by UV–vis spectroscopy, under CO, over the temperature range 318–343 K; the first-order rate constants given in Table 3 were obtained. The progress of each reaction was monitored by following the absorbance increase in the 365 nm band belonging to **3**. Figure 3 shows the spectral changes in the transformation **2** → **3**. The two clearly defined isosbestic points at 397 and 420 nm indicate that the isomerization is well-behaved and is free of kinetic complications. The absorbance versus time plot, depicted in the inset of Figure 3, shows the high quality of the least-squares fit of the 365 nm absorbance data to the growth of **3** by a first-order reaction. The effect of CO pressure (entries 2–4 in Table 3) and PPh₃ (entry 5) on the reaction was also explored, and no significant changes in the rate constant were observed, relative to the standard value reported for entry 2. The insensitivity of the rate constants to ligand additives and the Eyring activation parameters ($\Delta H^\ddagger = 21.6(3)$ kcal/mol; $\Delta S^\ddagger = -11(1)$ eu) both strongly support an intramolecular isomerization scenario that involves the migration of phosphine and CO groups about the cluster polyhedron. The details of these migrations were

(44) Park, B. K.; Miah, M. A.; Kang, H.; Lee, K.; Cho, Y.-J.; Churchill, D. G.; Park, S.; Choi, M.-G.; Park, J. T. *Organometallics* **2005**, 24, 675.

(45) Nesterov, V. N.; Watson, W. H.; Kandala, S.; Richmond, M. G. *Polyhedron* **2007**, 26, 3602.

(46) Watson, W. H.; Kandala, S.; Richmond, M. G. *J. Organomet. Chem.* **2007**, 692, 1648.

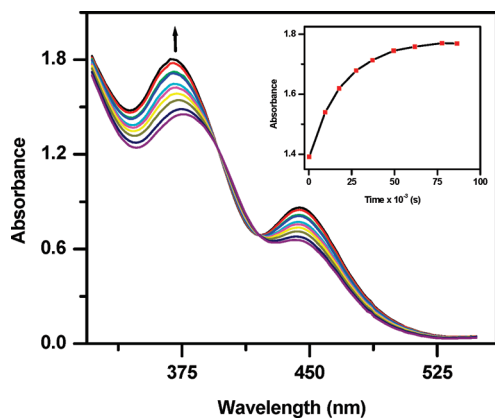


Figure 3. Representative UV-vis spectral changes for the isomerization **2** → **3** in toluene at 323 K under 1 atm of CO. The inset shows the absorbance versus time plot for the experimental data (□) and the nonlinear regression fit of the first-order rate constant k (solid black line).

investigated by the DFT calculations, the results of which are described in a subsequent section.

II. Reversible Ortho Metalation in 3 and Formation of $\text{HOs}_3(\text{CO})_9[\mu\text{-}1,2\text{-PhP}(\text{C}_6\text{H}_4\text{-}\eta^1)\text{C}_6\text{H}_4\text{PPh}_2]$ (4**).** As part of our ongoing studies of bond-activation processes, involving cluster-coordinated bidentate ligands,^{20–22,42,47–49} the origin and structural composition of the hydride cluster **4** that was isolated from the reaction between **1** and dppbz were next examined. While cluster **3** is thermally stable to CO loss at temperatures below 353 K, it is very sensitive to near-UV irradiation. Photolysis of a toluene solution containing **3**, using 366 nm light, led to CO loss and formation of **4**. The hydride-bridged cluster **4** could be obtained in quantitative yield, provided that the liberated CO was periodically removed through freeze-pump-thaw degas cycles or by active argon purge during irradiation.

In terms of the mechanism of formation of **4** from photolysis of **3**, optical excitation within the $\sigma \rightarrow \sigma^*$ manifold is expected to promote the formation of the putative, unsaturated cluster $\text{Os}_3(\text{CO})_9(\text{dppbz})$ through loss of one CO. This latter cluster is extremely sensitive to the presence of the released CO, which must be removed to avoid the regeneration of cluster **3**. Treatment of an isolated sample of **4** with CO (1 atm) overnight at 333 K in toluene led to the quantitative formation of **3**, thus establishing the reversible nature of the ortho metalation of the ancillary dppbz ligand. This reactivity paradigm appears to be general, in that several other activated diphosphine ligands have been shown by us to regenerate their respective $\text{Os}_3(\text{CO})_{10}(\text{P-P})$ cluster upon carbonylation.^{21,49}

4 was isolated in 88% yield after purification by column chromatography over alumina, followed by recrystallization. The presence of a bridging hydride at $\delta -16.43$ in the ^1H NMR spectrum and the pair of inequivalent doublets at $\delta 28.62$ and 39.54 in the ^{31}P NMR spectrum are in keeping with the formulated structure of **4**. Figure 4 shows the thermal ellipsoid plot of the molecular structure of **4**, as the CH_2Cl_2

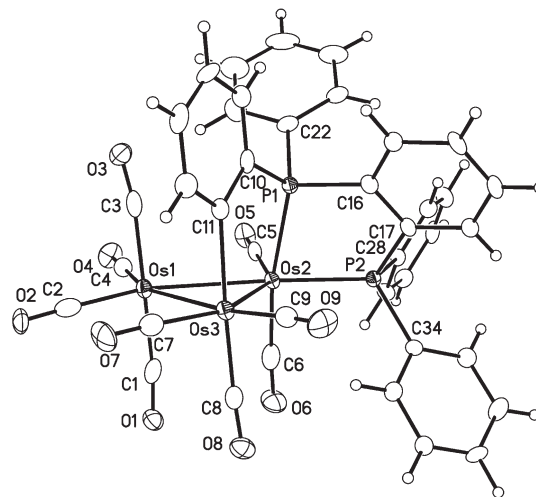


Figure 4. Thermal ellipsoid plot of **4**· CH_2Cl_2 at the 50% probability level with the hydrogen atoms shown as small spheres of arbitrary radii. The CH_2Cl_2 solvent has been omitted for clarity. Selected bond distances (Å) and angles (deg): Os(1)–Os(3) = 2.8808(4), Os(1)–Os(2) = 2.9330(3), Os(2)–P(2) = 2.323(1), Os(2)–P(1) = 2.367(2), Os(2)–Os(3) = 2.9948(4), Os(3)–C(11) = 2.184(6), P(1)···P(2) = 3.076(2); P(2)–Os(2)–P(1) = 81.94(5), P(2)–Os(2)–Os(1) = 172.92(4), P(1)–Os(2)–Os(1) = 97.55(4), C(16)–P(1)–Os(2) = 106.7(2), C(17)–P(2)–Os(2) = 109.4(2), C(17)–C(16)–P(1) = 118.1(4), C(16)–C(17)–P(2) = 116.2(4).

solvate, and confirms the ortho metalation of one of the aryl rings of the dppbz ligand. **4** contains 48e and is electronically saturated, assuming that the ancillary $\text{PhP}(\text{C}_6\text{H}_4\text{-}\eta^1)\text{C}_6\text{H}_4\text{PPh}_2$ ligand functions as a 5e-donor group. The Os–Os bond lengths range from 2.8808(4) Å (Os(1)–Os(3)) to 2.9948(4) Å (Os(2)–Os(3)) and reveal a mean distance of 2.9362 Å that parallels those Os–Os bond distances reported for other Os_3 clusters. Both phosphine atoms are coordinated to the Os(2) center and display axial (P(1)) and equatorial (P(2)) dispositions. The bridging hydride was not located during structural refinement, but it may be confidently assigned to the Os(2)–Os(3) bond, on the basis of the elongated distance of this bond, relative to the other two Os–Os bonds, and the stereochemical disposition of the C(9)O(9) and P(2) groups about the cluster polyhedron.⁵⁰ Here the Os(2)–Os(3)–C(9) and Os(3)–Os(2)–P(2) angles of 117.6(2) and 114.87(3)°, respectively, are significantly expanded from the idealized value of ca. 90° typically found for equatorial substituents in triangular clusters, due to the presence of the ancillary hydride.⁵¹ The Os(3)–C(11) bond distance of 2.184(6) Å is comparable to the Os–C bond distance found in the triosmium clusters $\text{H}_2\text{Os}_3(\text{CO})_9(\mu\text{-C}_6\text{H}_4\text{PPh})$, $\text{HOs}_3(\text{CO})_9(\text{PPh}_3)(\mu\text{-SbPh}_2)(\mu\text{-C}_6\text{H}_4)$, and $\text{Os}_3(\text{CO})_9[\mu\text{-PPh}(\text{C}_6\text{H}_4)\text{CH}_2\text{PPh}]$, each of which possess an activated aryl moiety.⁵²

(50) (a) Mingos, D. M. P.; Wales, D. J. *Introduction to Cluster Chemistry*; Prentice Hall: Englewood Cliffs, NJ, 1990. (b) Teller, R. G.; Bau, R. *Struct. Bonding (Berlin)* **1981**, 41, 1.

(51) (a) Churchill, M. R.; Hollander, F. J.; Lashewycz, R. A.; Pearson, G. A.; Shapley, J. R. *J. Am. Chem. Soc.* **1981**, 103, 2430. (b) Churchill, M. R.; Hollander, F. J. *Inorg. Chem.* **1981**, 20, 4124.

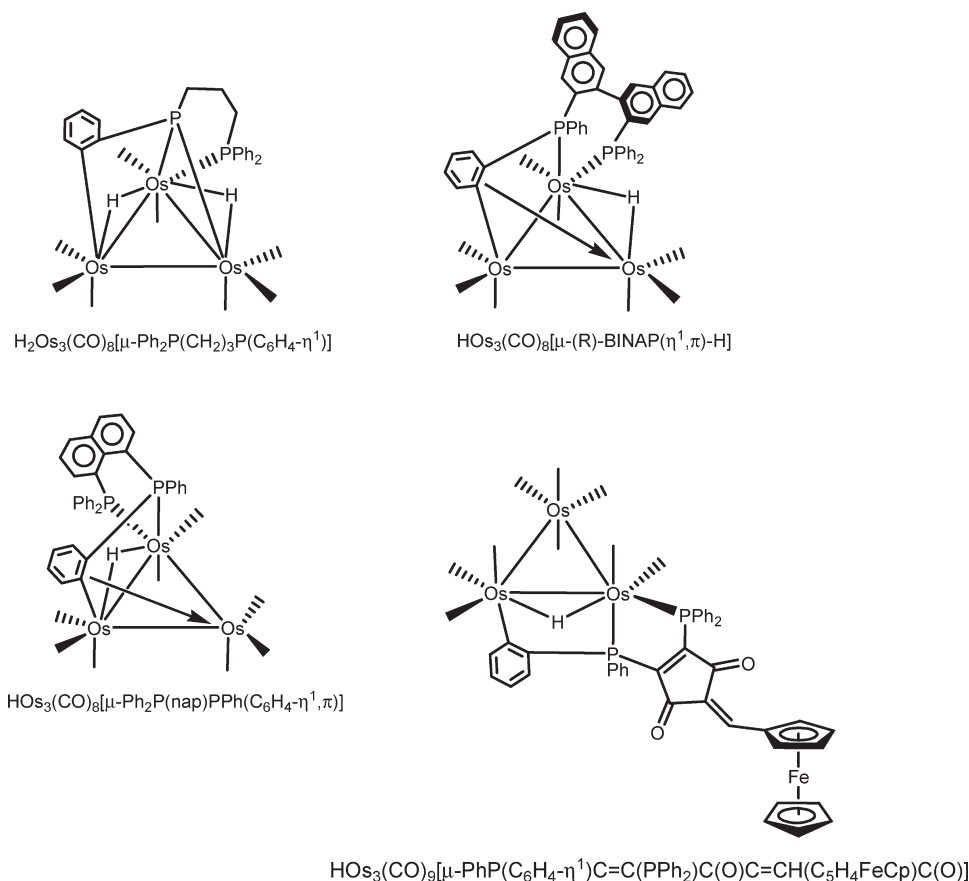
(52) (a) Colbran, S. B.; Irele, P. T.; Johnson, B. F. G.; Lahoz, F. J.; Lewis, J.; Raithby, P. R. *Dalton Trans.* **1989**, 2023. (b) Chen, G.; Deng, M.; Lee, C. K.; Leong, W. K. *Organometallics* **2002**, 21, 1227. (c) Kabir, S. E.; Miah, M. A.; Sarker, N. C.; Hussain, G. M. G.; Hardcastle, K. I.; Nordlander, E.; Rosenberg, E. *Organometallics* **2005**, 24, 3315.

(47) Poola, B.; Carrano, C. J.; Richmond, M. G. *Organometallics* **2008**, 27, 3018.

(48) Kandala, S.; Hammons, C.; Watson, W. H.; Wang, X.; Richmond, M. G. *Dalton Trans.* **2010**, 39, 1620.

(49) Huang, S.-H.; Keith, J. M.; Hall, M. B.; Richmond, M. G. *Organometallics* **2010**, 29, 4041.

Scheme 2



Decarbonylation of other 1,1- $\text{Os}_3(\text{CO})_{10}(\text{P-P})$ clusters, followed by ortho metalation of the diphosphine ligand, is observed upon heating; however, the composition of the resulting product is highly dependent upon the nature of the initial diphosphine, and further activation of the metalated aryl group is often found under harsh reaction conditions (i. e., refluxing toluene or heptane). A check of the Cambridge Structural Database (CSD version 5.31) for Os_3 clusters, possessing a chelating diphosphine that has experienced ortho metalation, reveals only four structures on file. Scheme 2 shows these four clusters, whose structural diversity is immediately obvious. Thermolysis of 1,1- $\text{Os}_3(\text{CO})_{10}(\text{dppp})$ in toluene under H_2 leads to the elimination of benzene and formation of the phosphido-bridged cluster $\text{H}_2\text{Os}_3(\text{CO})_8[\mu\text{-Ph}_2\text{P}(\text{CH}_2)_3\text{P}(\text{C}_6\text{H}_4\text{-}\eta^1)]$.⁵³ Heating the corresponding (*R*)-BINAP and dppn decarbonyl derivatives gives rise to the ortho-metalated products $\text{HOs}_3(\text{CO})_8[\mu\text{-(R)-BINAP}(\eta^1,\pi)\text{-H}]$ and $\text{HOs}_3(\text{CO})_8[\mu\text{-Ph}_2\text{P}(\text{nap})\text{PPh}(\text{C}_6\text{H}_4\text{-}\eta^1,\pi)]$, where the activated aryl ring in each product functions as a 7e face-capping donor ligand.^{54,55} Only $\text{HOs}_3(\text{CO})_9[\mu\text{-PhP}(\text{C}_6\text{H}_4)\text{C}=\text{C}(\text{PPh}_2)\text{C}(\text{O})\text{C}=\text{CH}(\text{C}_5\text{H}_4\text{FeCp})\text{C}(\text{O})]$, which was obtained as a ca. 1:1 mixture of diastereomers from the photolysis of 1,1- $\text{Os}_3(\text{CO})_{10}(\text{fbpcd})$ (where fbpcd = 2-(ferrocenylidene)-4,5-bis(diphenylphosphino)-4-cyclopenten-1,3-dione), exhibits a structure that is similar to that of **4**.^{21d}

III. Diphosphine Chelation in the Reaction of 1,2- $\text{Os}_3(\text{CO})_{10}(\text{MeCN})_2$ with dppbzF_4 . Treatment of **1** with a measured excess of dppbzF_4 at room temperature furnished 1,1- $\text{Os}_3(\text{CO})_{10}(\text{dppbzF}_4)$ (**6**) as the sole observable product, as assessed by ^{31}P NMR spectroscopy. Repeating the reaction at 0 °C in a sealed NMR tube afforded the same product, albeit more slowly. The inability to observe 1,2- $\text{Os}_3(\text{CO})_{10}(\text{dppbzF}_4)$ (**5**) spectroscopically indicates that the expected kinetic substitution product is unstable. Presumably, this instability is due to unfavorable steric interactions between the Ph_2P moieties and the ortho fluorines, interactions that are exacerbated by the coordination of the diphosphine ligand across the Os–Os bond.⁵⁶ The rapid isomerization of **5** to the thermodynamically more stable, diphosphine-chelated cluster **6** alleviates the strain in the “stretched” dppbzF_4 ligand. Scheme 3 summarizes the results of the reaction between **1** and dppbzF_4 .

6 was isolated in 85% yield after column chromatography over silica gel, followed by recrystallization, and it was characterized by IR and NMR spectroscopy, combustion analysis, and X-ray crystallography. The ^{31}P NMR spectrum revealed a diagnostic singlet at δ 34.00, while the ^1H NMR spectrum displayed three aromatic resonances at δ 7.20, 7.34, and 7.76 in a 4:8:8 integral ratio for the para, meta, and ortho hydrogens, belonging to the two PPh_2 moieties. The structure of **6**· $1/2$ (benzene) is shown in Figure 5, where the

(53) Deeming, A. J.; Hardcastle, K. I.; Kabir, S. E. *Dalton Trans.* **1988**, 827.

(54) Deeming, A. J.; Stchedroff, M. *Dalton Trans.* **1998**, 3819.

(55) Bruce, M. I.; Humphrey, P. A.; Schmutzler, R.; Skelton, B. W.; White, A. J. *Organomet. Chem.* **2004**, 689, 2415.

(56) For manifestations of the buttressing effect in chemical syntheses and the thermochemical properties of alkyl-substituted phenols, see: (a) Sammes, P. G.; Weller, D. J. *Synthesis* **1995**, 1205. (b) Choony, N.; Dadabhoy, A.; Sammes, P. G. *J. Chem. Soc., Perkin Trans. 1* **1998**, 2017. (c) Verevkin, S. P. *J. Chem. Thermodyn.* **1999**, 31, 1397.

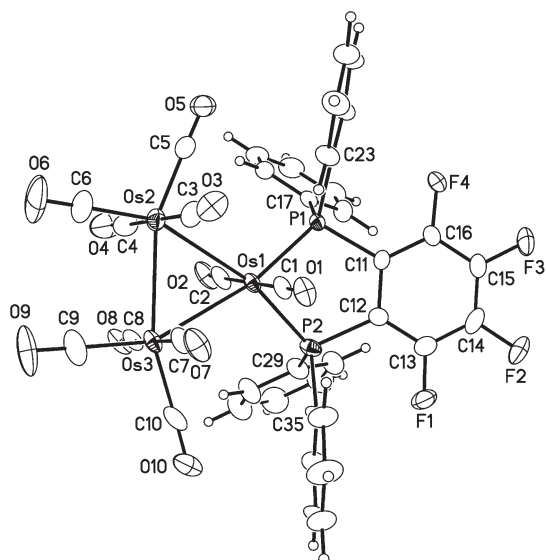
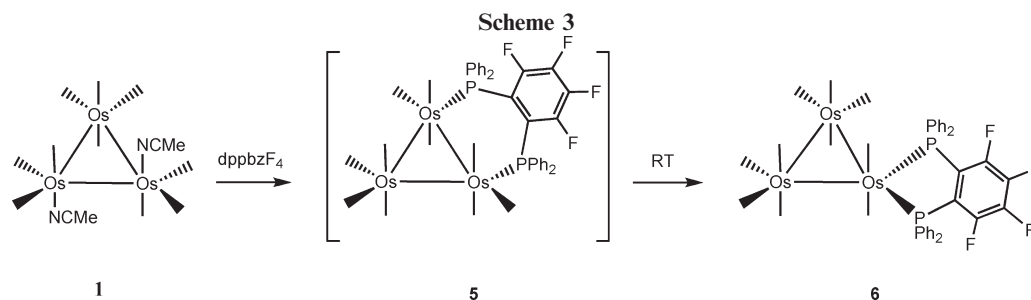


Figure 5. Thermal ellipsoid plot of one of the two independent molecules of $6 \cdot \frac{1}{2}C_6H_6$ at the 50% probability level. The hydrogen atoms are shown as small spheres of arbitrary radii, and the C_6H_6 solvent has been omitted for clarity. Selected bond distances (Å) and angles (deg): Os(1)–P(2) = 2.276(2), Os(1)–P(1) = 2.290(1), Os(1)–Os(2) = 2.8871(3), Os(1)–Os(3) = 2.9093(3), Os(2)–Os(3) = 2.8948(4), P(1)···P(2) = 3.106(2); P(2)–Os(1)–P(1) = 85.74(5), P(2)–Os(1)–Os(2) = 165.99(4), P(1)–Os(1)–Os(3) = 167.75(3), C(11)–P(1)–Os(1) = 107(1), C(12)–P(2)–Os(1) = 107.2(2), C(12)–C(11)–P(1) = 116.9(4), C(11)–C(12)–P(2) = 117.6(4).

presence of a chelating $dppbzF_4$ ligand is verified. The two independent molecules of **6** found in the unit cell do not exhibit any significant differences in geometries, and to our knowledge, the present example represents the first structurally characterized organometallic compound that contains the $dppbzF_4$ ligand.⁵⁷ The mean Os–Os bond distance in **6** is 2.8971 Å and is slightly shorter than the mean distance found for the Os–Os bonds in **3**. The ancillary aryl groups associated with the P(2) and P(3) atoms in the molecules of **6** are disordered over two positions. The observed bite angles for the chelating $dppzF_4$ ligands in the two independent molecules found in the crystal structure are 85.74(5) and 86.81(6)° for the P(1)–Os(1)–P(2) and P(3)–Os(4)–P(4) linkages and are similar to the 84.90(4)° bite angle observed in **3** for the $dppbz$ ligand.

IV. Synthesis and X-ray Diffraction Structure of $HOs_3(CO)_9[\mu-1,2-PhP(C_6H_4-\eta^1)C_6F_4PPh_2]$. The thermal and

(57) For a report on an iron complex containing the related ligand 1,2-bis(dimethylphosphino)tetrafluorobenzene, see: Higgins, S. J.; Jewiss, H. C.; Levason, W.; Webster, M. *Acta Crystallogr.* **1985**, *C41*, 695.

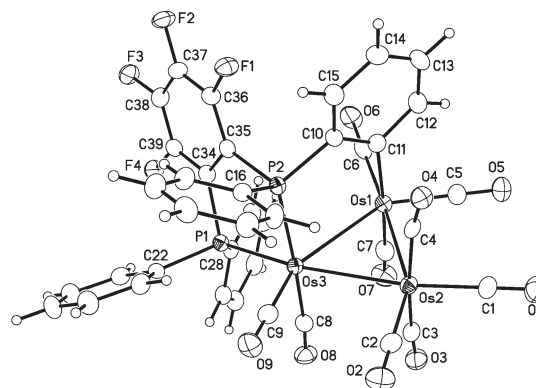


Figure 6. Thermal ellipsoid plot of $7 \cdot CHCl_3$ at the 50% probability level, with the carbon and hydrogen atoms shown as small spheres of arbitrary radii. The $CHCl_3$ solvent has been omitted for clarity. Selected bond distances (Å) and angles (deg): Os(1)–C(11) = 2.186(4), Os(1)–Os(2) = 2.8714(3), Os(1)–Os(3) = 2.9812(3), Os(2)–Os(3) = 2.9399(3), Os(3)–P(1) = 2.307(1), Os(3)–P(2) = 2.366(1), P(1)···P(2) = 3.139(2); P(1)–Os(3)–P(2) = 84.41(4), P(1)–Os(3)–Os(2) = 165.45(3), P(2)–Os(3)–Os(2) = 98.38(3), C(34)–P(1)–Os(3) = 108.6(1), C(35)–P(2)–Os(3) = 106.4(1), C(35)–C(34)–P(1) = 117.1(3), C(34)–C(35)–P(2) = 118.8(3).

photochemical properties of **6** were explored, in order to check whether there are any reactivity differences between it and **3**. **6** is stable to CO loss at 333 K but reacts in a manner identical with that of **3** under photolysis conditions (366 nm), to afford the corresponding hydride-bridged cluster **7**. Treatment of **7** with excess CO at 333 K regenerates **6** in quantitative yield. The ortho metalation of the ancillary diphosphine ligand occurs without complications, and the spectroscopic properties for **7** are consistent with the proposed structure

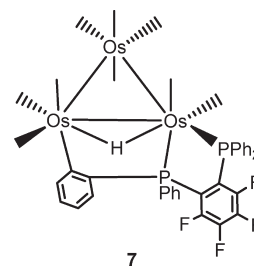


Figure 6 shows the thermal ellipsoid plot of $7 \cdot CHCl_3$, whose overall molecular architecture is compositionally similar to that of **4**. The Os–Os bond distances vary from 2.8714(3) Å (Os(1)–Os(2)) to 2.9812(3) Å (Os(1)–Os(3)), with the latter bond presumably serving as the locus for the bridging hydride that was not found during data reduction and refinement. The Os(1)–C(11) bond distance of 2.186(4)

Scheme 4

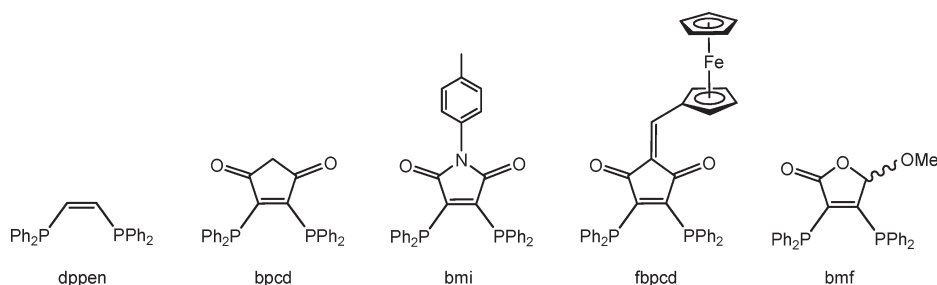


Table 4. Eyring Activation Data for the Isomerization of 1,2-Os₃(CO)₁₀(P-P) to 1,1-Os₃(CO)₁₀(P-P)

ligand	ΔH^\ddagger (kcal/mol)	ΔS^\ddagger (eu)	ref
dppen ^a	26.5(6)	-5(2)	21a
bpcd	25.0(7)	-2(2)	21b
bmi	24.0(1)	-5(1)	21c
fbpcd	23.1(3)	-7(1)	21d
dppbz	21.6(3)	-11(1)	this work
bmf ^a	26.9(7)	6(1)	unpublished

^aThe isomerization is reversible, and only the activation parameters for the forward portion of the reaction are reported.

A compares favorably to the corresponding Os–C bond distance found in **4**. The remaining bond distances and angles are unremarkable with respect to **4** and related osmium clusters characterized by our groups.

V. Possible Mechanisms for Diphosphine Isomerization in Os₃(CO)₁₀(P-P). The kinetics and activation parameters for the conversion **2** → **3** are in keeping with those found in related Os₃(CO)₁₀(P-P) clusters. Scheme 4 shows the different bidentate diphosphine ligands that have been examined and that undergo bridging to chelating isomerization in Os₃(CO)₁₀(P-P) clusters. Table 4 summarizes the Eyring data for the different diphosphine-substituted clusters. The data reveal a high degree of uniformity and strongly support a common mechanism for the isomerization of these diphosphine ligands about the Os₃ polyhedron, namely a nondissociative, first-order reaction, whose rate depends only on the Os₃(CO)₁₀(P-P) cluster.

As already noted, the dppbzF₄ ligand is atypical, inasmuch as the expected ligand-bridged cluster **5** was not observed when **1** was allowed to react with dppbzF₄. Instead, only the chelated isomer **6** was observed. This finding suggests that the enthalpy of activation for the rearrangement of **5** to **6** is lower than the enthalpies of activation, given in Table 4, for the rearrangements of all of the other Os₃(CO)₁₀(P-P) clusters in the table. The data in Table 4 allow one to estimate that $\Delta H^\ddagger < 20$ kcal/mol for the rearrangement of **5** to **6**.

The migration of P in the bridging-to-chelating transformation of the ancillary diphosphine ligand in Os₃(CO)₁₀(P-P) must be accompanied, at a minimum, by the permutation of at least one CO group between adjacent osmium centers. Two scenarios can account for the phenomenologically observed diphosphine isomerization in these molecules. The first scenario involves a pairwise exchange of a CO with

one of the phosphorus atoms across one of the Os–Os vectors. The second mechanism consists of a merry-go-round migration of two CO groups and one of the phosphorus atoms about the equatorial plane of the cluster.⁵⁸ Both mechanistic possibilities draw on established paradigms for CO fluxionality in polynuclear clusters,⁵⁹ and each isomerization process requires the formation of a nonclassical, bridging phosphorus atom along the reaction coordinate, during the transit of phosphorus across an Os–Os bond.⁶⁰

Entry into the pairwise exchange process mandates the presence of an axially disposed phosphine moiety, prior to the simultaneous migration of this phosphine and a trans axial CO group across a connecting Os–Os bond. The isomerization of a phosphine moiety from its initial equatorial site (**e**) in the bridged isomer (**B**) to an axial position (**a**) could be achieved by exchange between Os₁ and Os₃ of two axial CO groups, situated on opposite sides of the three-membered Os ring.^{61,62} The exchange mechanism requires conrotation of the other four substituents that lie

(59) For reports that deal with the elucidation of reaction mechanisms in polynuclear clusters using DFT calculations, see: (a) Persson, R.; Monari, M.; Gobetto, R.; Russo, A.; Aime, S.; Calhorda, M. J.; Nordlander, E. *Organometallics* **2001**, *20*, 4150. (b) Abdul Mottalib, M.; Begum, N.; Tareque Abedin, S. M.; Akter, T.; Kabir, S. E.; Arzu Miah, M.; Rokhsana, D.; Rosenberg, E.; Golzar Hossain, G. M.; Hardcastle, K. I. *Organometallics* **2005**, *24*, 4747. (c) Musaev, D. G.; Nowroozi-Isfahami, T.; Morokuma, K.; Rosenberg, E. *Organometallics* **2005**, *24*, 5973. (d) Musaev, D. G.; Nowroozi-Isfahami, T.; Morokuma, K.; Abedin, J.; Rosenberg, E.; Hardcastle, K. I. *Organometallics* **2006**, *25*, 203. (e) Li, Q.-S.; Xu, B.; Xie, Y.; King, R. B.; Schaefer, H. F. *Dalton Trans.* **2007**, 4312. (f) Cabeza, J. A.; Pérez-Carreño, E. *Organometallics* **2008**, *27*, 4697. (g) Cabeza, J. A.; del Río, I.; Fernández-Colinas, J. M.; Pérez-Carreño, E.; Sánchez-Vega, M. G.; Vázquez-García, D. *Organometallics* **2009**, *28*, 1832. (h) Cabeza, J. A.; Fernández-Colinas, J. F.; Pérez-Carreño, E. *Organometallics* **2009**, *28*, 4217. (i) Cabeza, J. A.; Van der Maelen, J. F.; García-Granda, S. *Organometallics* **2009**, *28*, 3666. (j) Cabeza, J. A.; del Río, I.; Goite, M. C.; Pérez-Carreño, E.; Pruneda, V. *Chem. Eur. J.* **2009**, *15*, 7339.

(60) A kinetically indistinguishable mechanism, involving the unsaturated cluster Os₃(CO)₁₀(η¹-P-P), formed through the dissociation of one arm of the diphosphine ligand from 1,2-Os₃(CO)₁₀(P-P), cannot be completely eliminated from consideration. However, given the rigid nature and syn disposition of the diphosphine ligands depicted in Scheme 4 and the uniformly negative entropies of activation in Table 4, this alternative does not seem likely.

(61) The isomerization of a phosphine moiety from an equatorial site to an axial site in the bridged isomer could, in principle, also be achieved by a 90° trigonal twist of the four substituents at one osmium center. However, in Os₃(CO)₁₂, the activation barrier for the 90° trigonal-twist pathway is computed to be 5.4 kcal/mol higher in energy than the type of isomerization process depicted in eq 3 involving exchange of trans diaxial CO molecules between adjacent Os atoms. The 5.4 kcal/mol lower energy of activation that is computed for the isomerization mechanism in eq 3 is consistent with the VT NMR data reported for CO exchange in Os₃(CO)_{12-x}P_x (where x = 1–4) and related clusters. In these clusters carbonyl scrambling preferentially occurs by exchanges of pairs of CO molecules between adjacent Os atoms, rather than by localized, 90°, tripodal, ligand rotations at a single Os metal center.⁶²

(58) In theory, these two isomerization mechanisms may be differentiated on the basis of the temperature-dependent behavior of the ancillary CO ligands in 1,2-Os₃(CO)₁₀(P-P). Unfortunately, global CO scrambling has been found to be competitive with the phosphine migration process, negating a mechanistic distinction by VT ¹³C NMR spectroscopy.

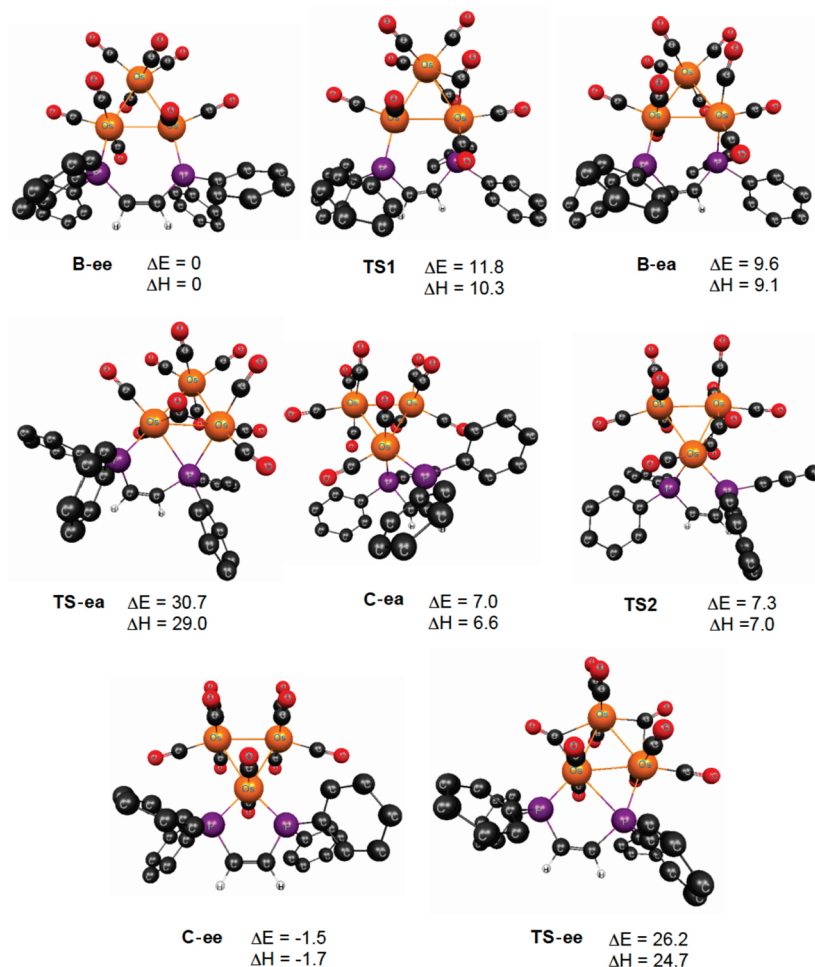
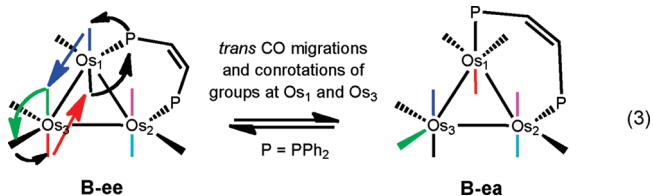


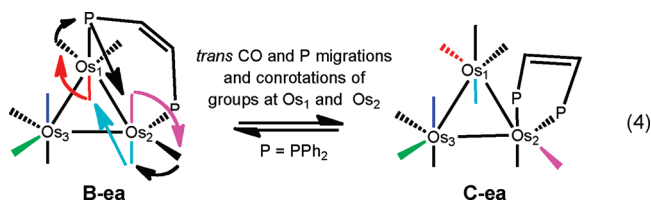
Figure 7. Optimized B3LYP structures for the intermediates and transition structures involved in the two-center and merry-go-round mechanisms for bridged to chelated isomerization reactions of $\text{Os}_3(\text{CO})_{10}(\text{dppen})$. ΔE and ΔH are given in kcal/mol, relative to **B-ee**.

approximately in the plane containing the two migrating CO groups and Os_1 and Os_3 . Equation 3 illustrates the ligand movements starting from bridged 1,2- $\text{Os}_3(\text{CO})_{10}[(Z)\text{-Ph}_2\text{PCH=CHPPH}_2]$ (**B-ee**). (The labeling scheme for the three osmium atoms is that employed in the ensuing discussion of the results of our DFT calculations, and the axial CO groups in eq 3 have been color-coded for clarity).

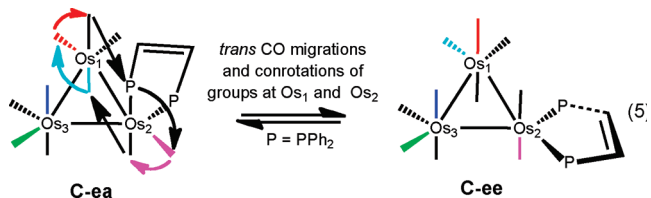


After the **B-ea** isomer has been formed, the axial phosphorus on Os_1 can migrate to Os_2 , concomitant with the migration of the axial CO, *trans* to the migrating phosphorus, from Os_2 to Os_1 . This process is fundamentally the same as that in eq 3, wherein the double migration again requires conrotation of axial and equatorial CO groups, but in this case at Os_1 and Os_2 . The migrations, rotations, and

resulting permutations of the groups attached to these two osmium atoms are shown schematically in eq 4.



Following the *trans* CO and P migrations in eq 4, the **C-ea** product is a chelated isomer; however, it has one phosphorus axial and the other equatorial, whereas, 1,1- $\text{Os}_3(\text{CO})_{10}[(Z)\text{-Ph}_2\text{PCH=CHPPH}_2]$ and all the other chelated diphosphines that have been isolated have both phosphorus atoms equatorial (**C-ee**). However, as shown in eq 5, a mechanism, similar to those in eqs 3 and 4 and involving migrations between Os_1 and Os_2 of a pair of *trans* diaxial CO groups, would put both of the phosphine groups that are attached to Os_2 in equatorial positions.



(62) (a) Deeming, A. J.; Donovan-Mtunzi, S.; Kabir, S. E. *J. Organomet. Chem.* **1985**, *281*, C43. (b) Alex, R. F.; Pomeroy, R. K. *Organometallics* **1987**, *6*, 2437.

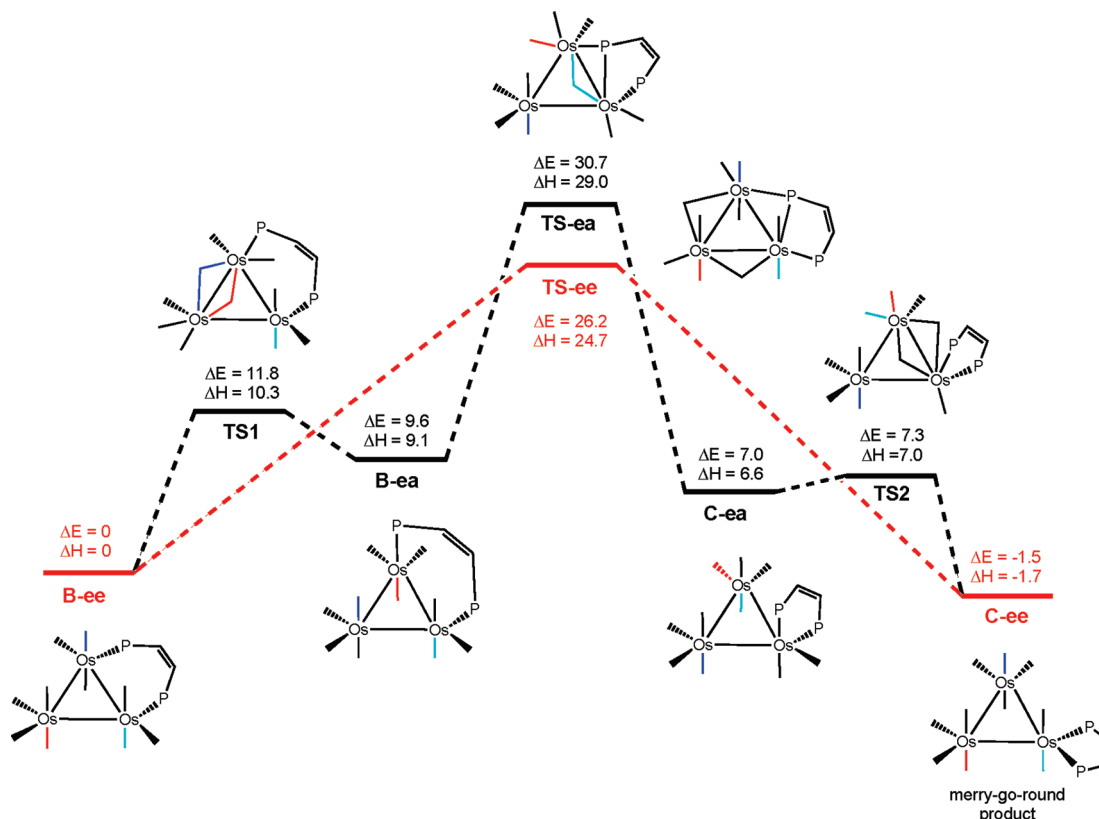
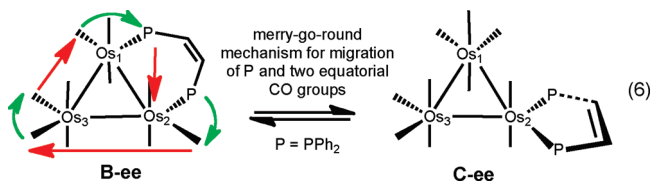


Figure 8. Potential energy surface for the conversion of **B-ee** to **C-ee** via in-plane (pairwise) migration and merry-go-round processes (where P = PPh₂). ΔE and ΔH are given in kcal/mol, relative to **B-ee**.

The mechanism that involves a merry-go-round migration of two CO groups and one of the phosphorus atoms in the equatorial plane of the **B-ee** cluster is shown in eq 6. This mechanism achieves in one step, involving the simultaneous migration of three equatorial groups, what takes three separate steps in the mechanism that involves the pairwise exchange of a CO and one of the phosphorus atoms (eq 4). However, the simplicity and economy of the merry-go-round mechanism in eq 6 does not, of course, necessarily make it the energetically preferred mechanism.



VI. Calculations of the Mechanisms and Barrier Heights for Diphosphine Isomerization in Os₃(CO)₁₀(P-P). We decided to use the results of electronic structure calculations to determine which of the above mechanisms is favored in the rearrangements of Os₃(CO)₁₀(P-P) clusters. As a test of our computational prediction of the preferred mechanism, we could assess how well the barrier heights, computed for the preferred mechanism, would reproduce the experimental activation enthalpies in Table 4. If the results of our calculations were thus validated, we could then use them to attempt to understand the observed variations in barrier heights with the structures of the phosphine ligands. For example, we could address the question of why replacement of the etheno group in dppe by the benzo group in dppbz lowers the

barrier to rearrangement of **2** to **3** by 5 kcal/mol and why fluorination of the benzo group apparently effects an even larger reduction in the enthalpy of activation, as evidenced by our failure to detect **5** as an intermediate in the formation of **6**.

Our computational studies were initiated by performing DFT calculations on the mechanism of the rearrangements of bridged to chelated Os₃(CO)₁₀(P-P) clusters, using dppe as the diphosphine ligand. The mechanism involving the pairwise exchange of a P and a CO ligand was studied first. Optimized geometries of the two stereoisomers of the bridged cluster 1,2-Os₃(CO)₁₀[(Z)-Ph₂PCH=CHPPh₂] were obtained: one stereoisomer, **B-ee**, with both phosphorus atoms equatorial, and the other stereoisomer, **B-ea**, with one phosphorus equatorial and the other axial. **B-ea** was computed to be higher in enthalpy than **B-ee** by 9.1 kcal/mol (the energies and all of the geometrical parameters of the minima and transition structures are given in the Supporting Information).

The mechanism for isomerization of **B-ee** to **B-ea** in eq 3 involves the pairwise exchange of the trans diaxial CO groups across the Os₁–Os₃ bond, accompanied by conrotation of four other substituents that are attached to these two osmium atoms.⁶¹ The transition structure (**TS1**) is the doubly CO bridged species shown in Figure 7. The barrier height for the mechanism in eq 3 was computed to be 10.3 kcal/mol, only 1.2 kcal/mol higher than the enthalpy of the **B-ea** isomer.

As shown in eq 4, the bridged intermediate **B-ea** can be transformed into the chelated structure **C-ea** by the pairwise exchange of axial CO and phosphine groups across the Os₂–Os₁ bond, concomitant with conrotation of the other

four groups that lie approximately in the same plane as the two migrating groups and the two osmium atoms to which they are attached. The transition structure (**TS-*ea***) for this process was located, and its structure is given in Figure 7. As shown in Figure 8, **TS-*ea*** is calculated to be 29.0 kcal/mol higher in enthalpy than **B-*ee*** and 18.7 kcal/mol higher than **TS1**. **TS-*ea*** is the highest transition structure in the isomerization of **B-*ee*** to **C-*ee*** by the three-step mechanism in eqs 3–5.

TS1 and **TS-*ea*** are both doubly bridged. Why is the latter transition structure computed to be so much higher in enthalpy than the former? Part of the reason is that passage from **B-*ea*** back to **B-*ee*** via **TS1** is more exothermic than passage from **B-*ea*** to **C-*ea*** by 6.6 kcal/mol, but this difference can be only a small contributor to the 18.7 kcal/mol difference between the two transition structures.

We believe that most of the difference is caused by the fact that in **TS1** both of the bridging groups are carbonyls; the presence of an empty π^* MO in an η^1 terminal CO group makes it easy for the carbonyl to accept a pair of electrons from an adjacent metal atom, to become an η^2 bridging carbonyl group. In contrast, a phosphine does not have such a low-energy, empty MO. This difference between carbonyl groups and phosphines is the reason bridging CO groups are common in transition-metal chemistry but bridging phosphines are not. It is the bonding of the phosphine group simultaneously to the Os₁ and Os₂ atoms in **TS-*ea*** that makes this transition structure much higher in energy than either **TS1** or **TS2**, in which both of the bridging ligands are CO.

Evidence in support of this explanation for the high energy of **TS-*ea***, relative to **TS1** and **TS2**, comes from bond lengths. For example, the CO that bridges in **TS-*ea*** has an average Os–C bond length that is only 0.204 Å longer in this transition structure than the average length of the Os–C bonds to this carbonyl group in **B-*ea*** and **C-*ea***. This is typical of the modest difference between the lengths of the Os–C bonds to the bridging carbonyl groups in **TS1**, **TS2**, and **TS-*ea*** and to the terminal carbonyl in **B-*ee***, **B-*ea***, and **C-*ea***. In contrast, the phosphine that bridges in **TS-*ea*** has an average Os–P bond length that is fully 0.355 Å longer in this transition structure than the average length of the Os–P bonds in **B-*ea*** and **C-*ea***.

As shown in Figure 8, **C-*ea*** is computed to have a 2.5 kcal/mol lower enthalpy than **B-*ea***. A barrier of only 0.4 kcal/mol is computed to separate **C-*ea*** from **C-*ee*** by doubly CO bridged **TS2**, which is below **B-*ea*** by 2.1 kcal/mol. The computed enthalpy difference of –1.7 kcal/mol between **B-*ee*** and **C-*ee***, in favor of the latter species, compares well with the experimentally determined ΔG° value of –1.4 kcal/mol that was obtained in our thermal equilibration studies on Os₃(CO)₁₀(dppn).^{21a}

There is a plethora of NMR reports on CO scrambling about triangular faces in polynuclear clusters.⁶³ Indeed, our calculations find **TS-*ee*** (Figure 8), the triply bridged transition structure for the one-step conversion of **B-*ee*** to **C-*ee*** in eq 6, to be 4.3 kcal/mol lower in enthalpy than **TS-*ea***, the highest energy transition structure for the three-step conversion of **B-*ee*** to **C-*ee*** via the mechanism in eqs 3–5. That

TS-*ee* is, indeed, a bona fide transition structure and not a short-lived intermediate on the PES for rearrangement of **B-*ee*** to **C-*ee*** was verified by normal-mode analysis, which found an imaginary frequency of 77i for **TS-*ee***. An IRC calculation confirmed that **TS-*ee*** does, in fact, connect **B-*ee*** directly to **C-*ee***.

It should be noted, however, that in Os₃(CO)₁₂, a *D*_{3h} structure with three bridging equatorial carbonyls is calculated to be ca. 5 kcal/mol higher in energy than a *C*_{2v} doubly bridged transition structure for exchanging a pair of trans diaxial carbonyl groups.⁶⁴ Therefore, at first it seems surprising that the preferred mechanism for the rearrangement of **B-*ee*** to **C-*ee*** is predicted to occur via the triply bridged, merry-go-round transition structure (**TS-*ee***), rather than by the doubly bridged transition structure for exchange of an axial phosphine and a trans axial CO between just two Os atoms (**TS-*ea***). Nevertheless, the results of the calculations by Li et al. on Os₃(CO)₁₂⁶⁴ and ours on Os₃(CO)₁₀[(*Z*)-Ph₂PCH=CHPh₂] are, in fact, wholly consistent with each other. As shown in Figure 8, although **TS-*ee*** is 4.3 kcal/mol lower in enthalpy than **TS-*ea***, 9.1 kcal/mol of the enthalpy of **TS-*ea*** comes from the enthalpy that is required to isomerize **B-*ee*** to **B-*ea***, so that the ligand exchange reaction can occur. Starting from **B-*ea***, the barrier to exchange of an axial phosphine and a trans axial CO via **TS-*ea*** is only $\Delta H^\ddagger = 19.9$ kcal/mol, which is 4.8 kcal/mol lower than $\Delta H^\ddagger = 24.7$ kcal/mol for exchange of three equatorial ligands via **TS-*ee***.

Unfortunately, the B3LYP/SDD calculations on Os₃(CO)₁₂ by Li et al. were performed without polarization functions in the D95 basis set.⁶⁴ Therefore, the barrier heights to rearrangement, computed by Li et al., are not directly comparable to the barrier heights for rearrangement of Os₃(CO)₁₀[(*Z*)-Ph₂PCH=CHPh₂], computed by us with the D95* basis set on phosphorus, oxygen, and carbon. In order to make meaningful comparisons between the barrier heights for rearrangement of these two molecules, we repeated the B3LYP/SDD calculations on Os₃(CO)₁₂ with the D95* basis set on phosphorus, oxygen, and carbon.

Our calculations on Os₃(CO)₁₂ found the energies of the doubly bridged *C*_{2v} and triply bridged *D*_{3h} transition structures to be respectively 13.0 and 17.7 kcal/mol higher than that of the *D*₃ equilibrium geometry. Both of these transition structure energies are 4.7 kcal/mol higher than the values published by Li et al. Clearly, inclusion of polarization functions in the basis sets for carbon and oxygen stabilizes the equilibrium geometry of Os₃(CO)₁₂ more than the transition structures for CO migrations in this molecule.

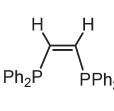
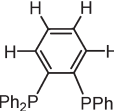
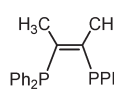
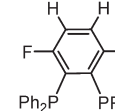
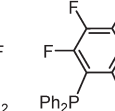
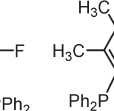
The energy $\Delta E = 13.0$ kcal/mol for the doubly bridged Os₃(CO)₁₂ transition structure, relative to the equilibrium geometry, is 8.1 kcal/mol smaller than $\Delta E = 21.1$ kcal/mol between **TS-*ea*** and **B-*ea***; the relative energy $\Delta E = 17.7$ kcal/mol for the triply bridged Os₃(CO)₁₂ transition structure is 8.5 kcal/mol smaller than $\Delta E = 26.2$ kcal/mol between **TS-*ee*** and **B-*ee***. Therefore, we believe that ca. 8 kcal/mol represents a reasonable estimate of the energetic penalty paid by Os₃(CO)₁₀[(*Z*)-Ph₂PCH=CHPh₂], relative to Os₃(CO)₁₂, for having a bridging phosphine in place of a bridging carbonyl group in the transition structures for ligand exchanges between both two and three Os atoms.⁶⁵

The calculated activation parameters of $\Delta H^\ddagger = 24.7$ kcal/mol and $\Delta S^\ddagger = -2.7$ cal/(mol K) for isomerization of **B-*ee*** to

(63) (a) Cotton, F. A. *Inorg. Chem.* **1966**, *5*, 1083. (b) Orlandi, A.; Frey, U.; Suardi, G.; Merbach, A. E.; Roulet, R. *Inorg. Chem.* **1992**, *31*, 1304. (c) Aime, S.; Dastrù, W.; Gobetto, R.; Krause, J.; Violano, L. *Inorg. Chim. Acta* **1995**, *235*, 357. (d) Besancon, K.; Laurenczy, G.; Lumini, T.; Roulet, R.; Bruyndonckx, R.; Daul, C. *Inorg. Chem.* **1998**, *37*, 5634. (e) Waterman, S. M.; Humphrey, M. G. *Organometallics* **1999**, *18*, 3116. (f) Canal, J. P.; Jennings, M.; Yap, G. P. A.; Pomeroy, R. K. *Dalton Trans.* **2008**, 1375.

(64) Li, Q.-S.; Xu, B.; Xie, Y.; King, R. B.; Schaefer, H. F. *Dalton Trans.* **2007**, 4312.

Table 5. Computed Energy and Enthalpy Differences between the Bridged and Chelated Os₃(CO)₁₀(diphosphine) Isomers and Computed Activation Energies and Enthalpies for the Bridged to Chelated Isomerization Reaction via the Merry-Go-Round Mechanism^d
Diphosphine Ligands

						
	a	b	c	d	e	f
ΔE	-1.5	-6.7	-8.2	-10.7	-11.2	-21.6
ΔH	-1.7	-6.7	-8.2	-11.1	-10.8	-21.5
ΔE^\ddagger	26.2	23.8	24.7	20.2	19.3	a
ΔH^\ddagger	24.7 ^b	22.5 ^c	23.6	18.9	18.2	a

^a Due to the size of and numbers of degrees of freedom in this ligand, no attempt was made to locate the transition structure for the rearrangement of the bridged to the chelated isomer. ^b The corresponding experimental value for entry a is $\Delta H^\ddagger = 26.5(6)$ kcal/mol. ^c The corresponding experimental value for entry b is $\Delta H^\ddagger = 21.6(3)$ kcal/mol. ^d All energies are in kcal/mol.

C-ee via triply bridged **TS-ee** are in good agreement with the experimental values (Table 4) of $\Delta H^\ddagger = 26.5(6)$ and $\Delta S^\ddagger = -5(2)$ cal/(mol K).^{21a} This agreement provides support for the computational finding that the one-step, merry-go-round mechanism in eq 6 really is preferred to the three-step mechanism in eqs 3–5 for the rearrangement of **B-ee** to **C-ee**. As discussed in section VII, further evidence comes from the good agreement of the activation parameters, calculated for the rearrangements via merry-go-round transition structures of Os₃(CO)₁₀(P-P) complexes, containing other diphosphine ligands (Table 5), with the values obtained experimentally (Table 4).

VII. Computed Reactivity Trends as a Function of the Ancillary Diphosphine Ligand in Isomeric Os₃(CO)₁₀(P-P) Clusters. Having established computationally that the merry-go-round scenario is the operative mechanism for the isomerization, from bridging to chelating, of the diphosphine ligand in 1,2- and 1,1-Os₃(CO)₁₀[(Z)-Ph₂PCH=CHPh]₂, we computed the energetics associated with this mechanism for the isomerization of other rigid diphosphine ligands about the triosmium cluster. The results of these calculations are summarized in Table 5. All of the isomerization reactions are computed to be exothermic. The calculated ΔH values for the isomerizations display more than an order of magnitude difference, ranging from $\Delta H = -1.7$ kcal/mol for the dppen ligand (entry **a**) to $\Delta H = -21.5$ kcal/mol for the highly substituted 1,2-bis(diphenylphosphino)-2,3,4,5-tetramethylbenzene ligand (entry **f**).

The calculated activation enthalpies range from $\Delta H^\ddagger = 24.7$ kcal/mol for the dppen ligand to $\Delta H^\ddagger = 18.2$ kcal/mol for the dppbzF₄ ligand (entry **e**), the most highly substituted diphosphine that has been studied experimentally. The computed value of $\Delta H^\ddagger = 22.5$ kcal/mol for the isomerization of **2** to **3** (entry **b** in Table 5) agrees well with the value of $\Delta H^\ddagger = 21.6(3)$ kcal/mol, measured in the current study (Table 4). Upon perfluorination of the benzo group, the enthalpy of activation for rearrangement is computed to decrease by 4.3 kcal/mol for the isomerization of **5** to **6** (entry **e** in Table 5).

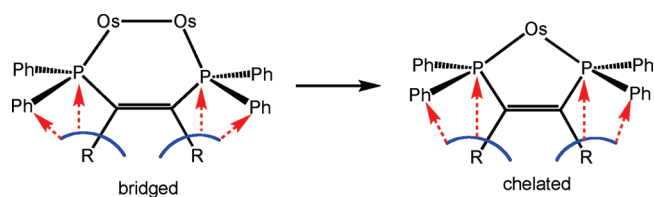


Figure 9. Schematic depiction of how, on going from the bridged to the chelated isomer, the decrease in P–C–C bond angle and the concomitant increase in the R–C–P angle reduce the steric interactions between each phosphorus atom and the phenyl groups attached to it with the R group that is bonded to the same carbon atom as the phosphorus.

The size of this decrease is consistent with our conjecture that the reason only chelated isomer **6** was observed in the reaction between **1** and dppbzF₄ is that **5** rearranges to **6** too quickly to be detected in our experiments.

The computational results in Table 5 underscore the influence that steric effects within the diphosphine ligands have on both the thermodynamics and kinetics of these isomerization reactions. As already discussed in section I, in connection with the X-ray structures of **2** and **3**, the rearrangement of the former to the latter decreases the C–C–P bond angle from ca. 126° in the six-membered ring of **2** to ca. 117° in the five-membered ring of **3**. Similar sized reductions in these internal angles are calculated to occur in the rearrangements of the bridged to the chelated isomers for all of the ligands in Table 5 (see the Supporting Information for the optimized structures). As shown schematically in Figure 9, decreasing the C–C–P bond angle and, concomitantly, increasing the R–C–P angle reduce the strain that is engendered by steric interactions between each phosphorus atom and the phenyl groups attached to it with the group, R, that is bonded to the same carbon as the phosphorus. Consequently, as the size of the R group increases, so does the amount of strain relieved by the rearrangement of the bridged to the chelated isomer, and as might be anticipated, the increased exothermicity of this reaction lowers the height of the barrier to it.

The effective size of the R group increases from left to right across Table 5, from R = H in entry **a** to R = C–CH₃ for the *o*-methyl groups in entry **f**, and the exothermicity of the conversion of the bridged to the chelated isomer also

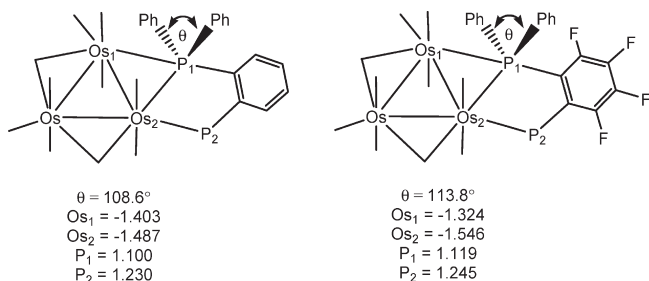
(65) We find that a similar energetic penalty of ca. 8 kcal/mol is incurred when the PH₃ group in Os₃(CO)₁₁(PH₃) replaces a bridging CO in Os₃(CO)₁₂ in the two-center and three-center transition structures for rearrangement.

increases in magnitude across Table 5. An exception to this trend is provided by entries **d** and **e**, where the two additional fluorines in the meta positions of entry **e** have little effect on the exothermicity of the rearrangement. This fact provides evidence that the exothermicity of the rearrangements of both of these fluorinated ligands is due to steric effects from the *o*-fluorines, rather than to electronic factors.

To the extent that the steric interactions between the geminal R and PPh₂ groups in the bridged isomer decrease, not only in the chelated isomer but also in the transition structure leading to it, one might expect the barrier heights to decrease with the size of R and, hence, with the increase in the magnitude of the exothermicity of the rearrangement.⁶⁶ An exception to the correlation between increased exothermicity and decreased barrier height is R = CH₃ (entry **c**). Although the exothermicity of the rearrangement of entry **c** is computed to be 1.5 kcal/mol greater than that of entry **b** (R = C–H), the barrier to the rearrangement of entry **c** is actually computed to be 1.1 kcal/mol higher than that of entry **b**. Apparently the methyl groups in entry **c** undergo some small destabilizing interactions in the transition structure for rearrangement that are absent in the chelated product.

If the increase in exothermicity and decrease in barrier height in Table 5 both have their origin in relief of strain in the bridged reactant, the effect of the size of R should have a larger influence on the exothermicity than on the barrier height. For example, the 9.1 kcal/mol calculated increase in exothermicity from entry **a** to entry **e** is accompanied by only a 6.9 kcal/mol decrease in barrier height. As would be expected, relief of the strain that is present in the bridged reactant is less complete in the transition structure leading to the chelated product than in the chelated product itself.

(66) A reviewer has suggested that charge effects, as opposed to steric effects, may be important in the transition state of our isomerization reactions, especially for the dppz and dppzF₄ ligands. With the *o*-(Ph₂P)₂C₆F₄ ligand, the migrating phosphine (P₁) shows evidence for enhanced rehybridization in the TS, in order to help relieve the steric interaction between the P₁Ph₂ group and the adjacent fluorine (the Ph–P₁–Ph angle is 113.8° in the dppbzF₄ TS vs 108.6° in the dppbz TS, as illustrated below). This angular change leads to a flattening of P₁, and this allows it to bond to Os₂ more strongly in the dppbzF₄ TS than in the dppbz TS, as shown by Os₂–P₁ bond lengths of 2.75 Å and 3.05 Å, respectively (see the Supporting Information). The additional electron donation from the P₁Ph₂ group in the dppbzF₄ TS makes Os₂ more negative than in the dppbz TS (–1.546 vs –1.487). Although P₁ is slightly more positive in the former TS than in the latter (1.119 vs 1.100), most of the positive charge that one might have expected to find on P₁ seems to be neutralized by the transfer of electrons from Os₁ back to P₁. The charges on Os₁ are respectively –1.324 and –1.403 in the dppbzF₄ TS and dppbz TS. Since the NBO charges for the bridged and chelated isomers of the dppz- and dppzF₄-substituted clusters reveal no significant differences, NBO differences in the TS charges are best viewed as arising from the rehybridization that accompanies the P₁ atom in the dppzF₄ TS, relative to the dppz TS, as influenced by the neighboring fluorine atom.



Conclusions

The synthesis and characterization of new dppbz- and dppbzF₄-substituted triosmium decacarbonyl clusters are reported, and the rate of conversion of bridged 1,2-Os₃(CO)₁₀(dppbz) (**2**) to chelated 1,1-Os₃(CO)₁₀(dppbz) (**3**) has been measured over a 25 °C temperature range. The slightly negative entropy of activation supports a nondissociative mechanism for the isomerization process.

The results of DFT calculations indicate that a merry-go-round mechanism, involving the concerted exchange of CO and diphosphine ligands about the equator of the cluster polyhedron is the lowest energy pathway. The calculations confirm the ability of a tertiary phosphine to function in a nonclassical coordination mode and to simultaneously bind to adjacent metal centers in a bridging fashion. However, calculations of the barrier heights for pairwise exchange of axial ligands indicate the bridging by phosphorus provides considerably less stabilization than bridging by a carbonyl carbon. Comparison of the energies computed for P-bridged structures in Os₃(CO)₁₀[(Z)-Ph₂PCH=CHPh₂] and the corresponding doubly and triply CO bridged structures in Os(CO)₁₂ indicates an energy penalty of about 8 kcal/mol for P versus CO bridging.

Increasing the effective size of the substituent, R, that is attached to the same carbon as phosphorus in the diphosphine ligands is shown, by the results of both our experiments and our calculations, to increase the reactivity of the bridging diphosphine ligand in this genre of cluster compounds. DFT calculations also find that increasing the geminal substituent size has an even greater effect on increasing the exothermicity of the rearrangement of the bridged to the chelated isomer. These findings are attributed to the ca. 10° decrease in the C–C–P bond angle that occurs during the transformation of the six-membered ring in the bridged isomer to the five-membered in the chelated isomer and the concomitant increase in the R–C–P angle. Increasing the latter angle decreases the magnitude of the nonbonded interactions of phosphorus and the phenyl groups attached to it with the substituent that is attached to the same carbon. The larger the effective size of the substituent group, R, the larger is the amount of steric strain removed on the rearrangement of the bridged to the chelated isomer of Os₃(CO)₁₀(P–P).

Acknowledgment. Financial support from the Robert A. Welch Foundation (Grant B-0027 to W.T.B. and Grant B-1093 to M.G.R.) and from the National Science Foundation (to W.T.B.) is greatly appreciated. X.W. acknowledges support by the U.S. Department of Energy, Office of Science, under Contract No. DE-AC05-00OR22725 managed by UT Battelle, LLC. The NSF-MRI program grant CHE-0840518 is gratefully acknowledged for support of the NMR facilities at UNT. NSF support of the UNT computational facilities through grant CHE-0741936 is acknowledged. Preliminary experimental work conducted by Mr. Sean Hunt and preliminary calculations by Dr. Haiyan Wei are acknowledged.

Supporting Information Available: Text, figures, tables, and CIF files giving an Eyring plot of the dppbz isomerization data, atomic coordinates and energies of all optimized stationary points and transition states, NBO charges and selected bond distances for the merry-go-round TS structures containing dppz and dppzF₄ ligands, and crystallographic data. This material is available free of charge via the Internet at <http://pubs.acs.org>.